

ASYMPTOTIC-PRESERVING A POSTERIORI ANALYSIS OF DIFFUSION AND FLOW-MATCHING SAMPLERS

Shiheng Zhang
University of Washington
shzhang3@uw.edu

ABSTRACT

Diffusion and flow-matching samplers integrate a learned probability-flow ODE from a large noise scale down to a small terminal floor σ_{\min} , at which the score is stiff and the flow develops a boundary layer. We treat σ_{\min} as a singular-perturbation parameter and determine which fixed-step samplers are *asymptotic-preserving* (AP)—stable and uniformly accurate as $\sigma_{\min} \rightarrow 0$ —casting the criteria as an *a posteriori audit*: residual functionals with σ_{\min} -uniform coefficients, computable on a pretrained checkpoint without ground-truth scores or exact trajectories. On the terminal layer, Euler in the σ -clock, the deterministic DDIM update, is the unique layer-exact discretization up to affine reparameterization, with rectified flow its flow-matching counterpart; the λ -clock is stable only for steps $h \leq h_* = 1 + W(1/e)$, and the uniform- σ^2 heat clock stalls a σ_{\min} -independent distance from the data. On two solvable models (rank-deficient Gaussian, symmetric two-point mixture), deterministic samplers remain first-order uniformly accurate with no $\log(1/\sigma_{\min})$ factor, even across a symmetric posterior-switching interface whose distributional budget is a universal constant; the logarithm is charged entirely to the Itô term of stochastic samplers, whose path-KL scales as Λ^2/N against the ODE’s $O(\Lambda^2/N^2)$ budget, $\Lambda = \log(\sigma_{\max}/\sigma_{\min})$. On the EDM CIFAR-10 checkpoint, spectra measured once predict held-out residual budgets across step count, schedule, and noise level against pre-specified gates with no per-configuration refitting, and calibrate the Itô coefficient at $\mathcal{M}_1 = 1.00 \pm 0.01$. The clock decides stability; the noise, not the geometry, charges the logarithm.

1 INTRODUCTION

Diffusion and flow-matching models sample by integrating a learned field from noise down to data, stopping at a small but nonzero terminal noise scale: EDM (Karras et al., 2022) uses $\sigma_{\min} = 0.002$. The stop is structural: as $\sigma_{\min} \rightarrow 0$ the score becomes stiff, its Lipschitz constant growing like σ_{\min}^{-2} (2.5×10^5 at the EDM floor). The floor is therefore a genuine singular parameter of the sampling problem, yet it is typically tuned by hand and excluded from the analysis, which either assumes a time-uniformly Lipschitz score or studies an early-stopped process whose iteration count grows like $\log(1/\sigma_{\min})$ (Chen et al., 2022; Benton et al., 2024; De Bortoli, 2022).

This paper analyzes the floor directly. Near the data the probability-flow ODE develops a *boundary layer*, the structure that asymptotic-preserving (AP) numerics was built to handle (Roos et al., 2008; Jin, 2022), and the appropriate criterion for a *fixed-step* sampler is stability and accuracy *uniform* in σ_{\min} . Written in the denoiser D and its normalized residual η , the samplers in use (deterministic, stochastic, and flow-matching) are a single flow traversed under different choices of *clock*, *gauge*, and noise level (§2), so the AP criterion reduces to a classification of traversal choices. Under this classification, empirical design wisdom on schedules, parameterizations, and stochasticity becomes a set of rigidity theorems, packaged as an *a posteriori audit* whose functionals are computable on a pretrained checkpoint (§3).

Stability on the pure terminal layer is characterized first (§4). A frozen-field Euler step is layer-exact if and only if its clock is affine in σ , which makes the σ -clock step, precisely DDIM (Song et al., 2020a), the unique fitted operator up to affine reparameterization, with rectified flow its flow-matching counterpart; the λ -clock is stable only below the Lambert- W threshold $h_* = 1 + W(1/e)$;

and the uniform- σ^2 heat clock cannot resolve the layer at all, stalling a σ_{\min} -independent distance from the data.

Accuracy beyond the linear regime follows. On the rank-deficient Gaussian model (§4.2), DDIM is first-order uniformly accurate: its only defect is a one-sided covariance contraction $-\log \rho \leq h/4$ with a σ_{\min} -free constant, and the schedule’s only remaining role is to resolve the data’s spectral band. The first nonlinearity—a symmetric posterior-switching interface (§5)—destroys pointwise accuracy but not distributional accuracy: its deterministic budget is a universal, σ_{\min} -independent constant, still with no logarithm.

The $\log(1/\sigma_{\min})$ cost arises only in the Itô term of stochastic samplers (§5). A horizon-extensive functional \mathcal{M}_1 yields $\text{KL} \sim \Lambda^2/N$ for the SDE against an $O(\Lambda^2/N^2)$ discretization budget for the ODE, already on rank-deficient Gaussian data and independently of any interface. These functionals of the learned field are measurable without a ground-truth score, and they are *predictive*: on a pretrained EDM CIFAR-10 checkpoint, spectra measured *once* forecast held-out residual budgets across step count, schedule, and noise level against pre-specified gates, with no per-configuration refitting; the Itô coefficient calibrates at $\mathcal{M}_1 = 1.00 \pm 0.01$ (§6).

Contributions. (i) An AP formulation of terminal-layer sampling and an a posteriori audit whose functionals carry σ_{\min} -uniform coefficients (§3); (ii) clock rigidity theorems calibrated by named constants—the threshold $h_* = 1 + W(1/e)$ and the Wallis floor $1/\sqrt{\pi}$ (Theorem 2), the tangential $1/4$ (Theorem 3); (iii) the assignment of the logarithm: a single symmetric switching interface charges the deterministic sampler only a universal constant, with matched interface tail $3\pi/16$ (Theorem 4), while the Itô term of stochastic samplers is horizon-extensive (Corollary 4); and (iv) a pre-specified predictive campaign in which spectra measured once on a pretrained checkpoint forecast held-out residual budgets with no refit (§6). In one line: *the clock decides stability; the noise, not the geometry, charges the logarithm.*

2 PRELIMINARIES: ONE FLOW, MANY SAMPLERS

Deterministic, stochastic, and flow-matching samplers share the same noised marginals $\{p_\sigma\}$ and denoiser/residual field, differing only in a clock, a scaling gauge, a noise level, and a frozen object. This section makes that precise and asks which choices stay stable and accurate as $\sigma_{\min} \rightarrow 0$.

The flow and its velocity. Sampling reverses a noising process. From data $X_0 \sim p_0$ on \mathbb{R}^D form $X_\sigma = X_0 + \sigma Z$, $Z \sim \mathcal{N}(0, I)$, with variance-exploding (VE) marginals $p_\sigma := \text{Law}(X_\sigma) = p_0 * \mathcal{N}(0, \sigma^2 I)$ (Song et al., 2020b; Karras et al., 2022); a sampler walks these marginals from $p_{\sigma_{\max}} \approx \mathcal{N}(0, \sigma_{\max}^2 I)$ (after centering, with σ_{\max} above the data scale) down to a terminal $p_{\sigma_{\min}}$. The one object a sampler must learn is the *denoiser* $D(x, \sigma) := \mathbb{E}[X_0 | X_\sigma = x] = x + \sigma^2 \nabla \log p_\sigma(x)$ —or, equivalently, any of its affine repackagings: the score (by Tweedie’s formula (Robbins, 1992; Efron, 2011)), the noise, or the velocity a given sampler regresses. The deterministic sampler follows the probability-flow ODE (PF-ODE), which, written first in the score and then through Tweedie, reads

$$\frac{dX}{d\sigma} = -\sigma \nabla \log p_\sigma(X) = \frac{X - D(X, \sigma)}{\sigma} =: \eta(X, \sigma), \quad \sigma : \sigma_{\max} \downarrow \sigma_{\min}. \quad (1)$$

The velocity of the flow is thus the normalized *residual* $\eta = (x - D)/\sigma$, equivalently the posterior noise $\eta(x, \sigma) = \mathbb{E}[Z | X_\sigma = x] = -\sigma \nabla \log p_\sigma(x)$, the noise-prediction variable native to diffusion (Song et al., 2020a; Albergo et al., 2025). Rearranged, the same identity splits the state into a data-scale part and a vanishing remainder,

$$x = D(x, \sigma) + \sigma \eta(x, \sigma), \quad (2)$$

and read against equation 1 the split is dynamical: the state is its posterior mean plus σ times the flow’s velocity, so the remainder $\sigma \eta = x - D$ measures departure from the data-scale estimate D . Being $O(\sigma)$, it decays as $\sigma \rightarrow 0$ —a terminal boundary layer (the singular limit below).

The split also fixes the bookkeeping. Since $X_\sigma = X_0 + \sigma Z$, the remainder $x - D$ is $O(\sigma)$ on p_σ -typical samples, so $\eta = O(1)$: neither D nor η is stiff as $\sigma \rightarrow 0$. The stiffness lives entirely in the score $= -\sigma^{-1}\eta$, of magnitude $O(\sigma^{-1})$ with normal Jacobian $O(\sigma^{-2})$, which is why every sampler

below is written in D and η , never the bare score. The denoiser’s own Jacobian is, by second-order Tweedie, the posterior covariance in units of σ^2 ,

$$J_D := \nabla_x D = I + \sigma^2 \nabla^2 \log p_\sigma = \frac{\text{Cov}[X_0 | X_\sigma = x]}{\sigma^2}, \quad (3)$$

which governs Sections 4–5 (in the Gaussian model of §4, $\|J_D\| \leq 1$; in a scalar reduction we write D_x for its single eigenvalue). The PF-ODE, however, is only one way to traverse the marginals $\{p_\sigma\}$.

Every sampler is a traversal choice. The stochastic samplers change only the noise level: they hold every marginal p_σ fixed while reinjecting noise. In the data-time $\lambda = \log(\sigma_{\max}/\sigma)$ the marginal-preserving VE family is

$$dX_\lambda = -(1 + \beta) \sigma_\lambda \eta(X_\lambda, \sigma_\lambda) d\lambda + \sqrt{2\beta} \sigma_\lambda dW_\lambda, \quad \beta \geq 0, \quad (4)$$

with $\beta = 0$ the PF-ODE equation 1 and $\beta = 1$ the canonical reverse SDE (Anderson, 1982; Song et al., 2020b); the factor $1 + \beta$ is what holds the marginals fixed,¹ and EDM churn (Karras et al., 2022) is a discrete instance. Flow-matching and stochastic-interpolant samplers (Lipman et al., 2022; Liu et al., 2022; Albergo et al., 2025) appear distinct: they push a Gaussian path $X_t = \alpha_t X_0 + \sigma_t Z$ (rectified flow takes $\alpha_t = 1 - t$, $\sigma_t = t$) by the velocity $v_t = \dot{\alpha}_t \mathbb{E}[X_0 | X_t] + \dot{\sigma}_t \mathbb{E}[Z | X_t]$ —but they change only the clock and the gauge: the rescaling $\tilde{X} := X_t/\alpha_t = X_0 + \sigma Z$ with $\sigma := \sigma_t/\alpha_t$ undoes the gauge and lands on the same marginals p_σ , with

$$v_t(x) = \dot{\alpha}_t D(\tilde{x}, \sigma) + \dot{\sigma}_t \eta(\tilde{x}, \sigma), \quad \tilde{x} = x/\alpha_t, \quad \sigma = \sigma_t/\alpha_t, \quad (5)$$

so a flow-matching sampler is the PF-ODE equation 1 in a reparameterized time and scale. In every case, then, the learned content is the single denoiser D (equivalently the residual η), and a sampler is that object plus a rule for traversing the noise scales: a clock, a scaling gauge α_t , a noise level β , and a *frozen object*, which repackaging of (D, η) is held fixed across a step (§3, Appendix E).

Clocks. Of these four traversal choices, the analysis turns on the *clock*: a monotone reparameterization $\tau = \phi(\sigma)$, which fixes the noise scales the steps land on. Besides the σ -clock ($\phi = \text{id}$) these are the λ -clock $\lambda = \log(\sigma_{\max}/\sigma)$, the *half* log-SNR of Lu et al. (2022); Zhang & Chen (2022);² the heat-clock $\tau = \sigma^2$ (the uniform noise-level time of the DDPM/VP lineage Song et al., 2020b, whose VE marginals solve a heat equation, Karras et al., 2022, App. B.5); and the flow-matching clock t via $\sigma = \sigma_t/\alpha_t$. We write $h_n = \log(\sigma_n/\sigma_{n+1}) > 0$ for the step and $\Lambda = \log(\sigma_{\max}/\sigma_{\min})$ for the horizon (the EDM loss weight is $w(\sigma)$).

The singular limit. As $\sigma_{\min} \rightarrow 0$ the score becomes stiff—normal Jacobian growing like σ^{-2} —and the PF-ODE equation 1 develops a *terminal layer*, the collapse implied by the split equation 2. In local normal coordinates $r = x - \pi_{\mathcal{M}}(x)$ about $\mathcal{M} = \text{supp } p_0$, the leading drift is r/σ (exactly so when \mathcal{M} is a linear subspace, and up to $O(\sigma)$ under the manifold model $D = \pi_{\mathcal{M}}(x) + O(\sigma^2)$), so $r(\sigma) \propto \sigma$ collapses onto the data: to leading order r is the remainder $\sigma\eta$, and the layer width is σ itself. This layer, with σ_{\min} the singular parameter, is what the AP criterion must control. Keeping η order one along the discretization, the estimate that survives the limit, is our stability requirement (E1, §3), and the question is the *asymptotic-preserving* (AP) one of singular-perturbation numerics (Roos et al., 2008; Jin, 2022): can a fixed-step sampler stay stable and consistent as $\sigma_{\min} \rightarrow 0$ without a step restriction degenerating like σ_{\min} ? The following sections answer it for the denoiser–residual samplers above.

3 THE ASYMPTOTIC-PRESERVING AUDIT

Section 2 reduced every sampler to four traversal choices—clock, gauge, noise level, frozen object—on the one learned pair (D, η) . The *audit*, given a pretrained network and a policy, is four residual functionals, each an expectation of η -increments, none requiring a ground-truth score, certify terminal stability and localize discretization cost in scale. Theorem 1 is the local law that defines them; its

¹Fixed by a variance check on a normal coordinate: dropping the factor lets the $\beta = 1$ variance miss σ^2 .

²Not the full log-SNR $\log(\alpha_t^2/\sigma_t^2)$: the factor of two would rescale every clock constant below.

corollaries give the integrated budgets, the N -scaling of deterministic against stochastic sampling, and the schedule-design hypotheses. The solvable models of §4–5 then calibrate each functional in closed form, and §6 measures the law on a real checkpoint and marks the boundary of what is certified.

Definition 1 (AP and uniform accuracy). A solver family Φ_h for equation 1 is (i) *AP-stable* if it admits a stability bound uniform in σ_{\min} , with no step restriction that degenerates as $\sigma_{\min} \rightarrow 0$; (ii) *AP-consistent* if, at fixed h , its $\sigma_{\min} \rightarrow 0$ limit is a consistent discretization of the limit flow (which projects onto $\text{supp } p_0$ and transports along it); and (iii) *uniformly accurate* (UA) of order p if, on an admissible mesh (maximal step $\leq h$), $W_2(\text{Law}(x_N), p_{\sigma_{\min}}) \leq C h^p$ with C independent of σ_{\min} .

Clauses (i)–(ii) ask discretization and the limit $\sigma_{\min} \rightarrow 0$ to commute (Jin, 2022); (iii) is the uniform accuracy they buy. The distributional metric is forced: pointwise trajectory accuracy is impossible, the limiting flow map being discontinuous (§5), while total variation and KL are vacuous against the lower-dimensional data support. Singular-perturbation numerics offers two mechanisms for σ_{\min} -uniformity (Roos et al., 2008): a *fitted mesh*, which grades nodes into the layer (schedule engineering, e.g. the EDM $\rho = 7$ power law (Karras et al., 2022), is of this kind) and a *fitted operator*, which builds the layer solution into the scheme so that any mesh works; the exponential integrators (Lu et al., 2022) are half of one, and §4 exhibits the σ -clock step as a full one, whereupon the schedule is demoted to a second-order concern (band resolution, not layer survival).

Definition 1, however, speaks of scheme *families* and exact flows. In practice one has a single checkpoint, a fixed schedule, one run, and no ground-truth score. The runtime interface is built from the only $O(1)$ coordinate the singular limit leaves standing.

The audit interface. Fix a mesh $\{\sigma_n\}_{n=0}^N$ with $\lambda_n = \log(\sigma_{\max}/\sigma_n)$, steps $h_n = \lambda_{n+1} - \lambda_n$, horizon Λ , and a policy (clock, gauge, noise level β , frozen object). Write $\eta_n = \eta(x_n, \sigma_n)$ along the discrete trajectory and $n(\lambda)$ for the active step at time λ . The audit’s outputs are the following functionals; all are expectations of η -increments, so each is read off the pretrained network, needing no ground-truth score or exact trajectory: only checkpoint evaluations on probe states.

Definition 2 (Audit functionals). (a) *Residual stability*. The certificate form asks that the normalized residual of equation 2 not be amplified across the run,

$$(E1) \quad \sup_{0 \leq n \leq N} \frac{\|\eta_n\|}{\|\eta_0\|} \leq C, \quad C \text{ independent of } \sigma_{\min}, N, \quad (6)$$

and we call a discretization *residual-AP* when it holds; the measured statistic is the population ratio $\hat{\mathcal{E}}_1(n) := \mathbb{E} \|\eta_n\| / \mathbb{E} \|\eta_0\|$. E1 certifies stability, not accuracy (Remark 3).

(b) *Residual path budget*. Per dimension, along the interpolated sampling process at noise level β ,

$$(E2) \quad \mathcal{E}_2(\{\lambda_n\}; \beta) := \frac{1}{D} \mathbb{E} \int_0^\Lambda \left\| \eta(X_\lambda, \lambda) - \eta(X_{\lambda_{n(\lambda)}}, \lambda_{n(\lambda)}) \right\|^2 d\lambda, \quad (7)$$

the expectation taken along the sampler’s own path law, hence measurable at runtime from dense substeps on pilot trajectories. Three objects share this symbol and must not be conflated: the marginal-faithful $\mathcal{E}_2^{\text{low}}$ that the mesh laws price is the ODE’s L^2 discretization budget at $\beta = 0$ (no path-KL exists; Corollary 1(c)) and the SDE budget at $\beta > 0$, whereas the frozen-drift $\mathcal{E}_2^{\text{frozen}}$ is the Girsanov/KL-facing companion; flow and frozen differ by the $O(h)$ numerical-path substitution of Corollary 1(b) (§6, Appendix G).

(c) *Scale spectra*. With D_λ the material derivative along the deterministic flow, $D_\lambda \eta := \partial_\lambda \eta + ((D - x) \cdot \nabla_x) \eta$, and $m_1(\sigma) := D^{-1} \mathbb{E}_{p_\sigma} \|\eta\|^2$ the residual mass,

$$\mathcal{M}_{\text{det}}(\sigma) := \frac{1}{D} \mathbb{E}_{p_\sigma} \|D_\lambda \eta\|^2, \quad \mathcal{M}_1(\sigma) := \frac{1}{D} \mathbb{E}_{p_\sigma} \|I - J_D\|_{\mathbb{F}}^2. \quad (8)$$

Remark 1 (Operational forms; why Frobenius). E1 is free (the η_n are already computed); \mathcal{E}_2 and \mathcal{M}_{det} come from dense substeps on pilot runs; \mathcal{M}_1 from a *same- σ kick*: perturbing $x^+ = x + \sigma \sqrt{2\beta\tau} z$, $z \sim \mathcal{N}(0, I)$, at fixed σ gives

$$\mathbb{E}_z \|\eta(x^+, \sigma) - \eta(x, \sigma)\|^2 = 2\beta\tau \|I - J_D(x)\|_{\mathbb{F}}^2 + O(\tau^2), \quad (9)$$

functional	reads	certifies	cost
E1 equation 6	terminal residual amplification	stability (residual-AP); <i>not</i> accuracy	free
$\mathcal{E}_2^{\text{flow}}$ equation 7	η -increments, dense flow path	mesh budget (ODE L^2 /SDE)	substeps
$\mathcal{E}_2^{\text{frozen}}$	η -increments, frozen drift	path-KL, $\frac{(1+\beta)^2}{4\beta}$	substeps
\mathcal{M}_{det} equation 8	deterministic coefficient	localizes ODE cost; $\frac{1}{3}\mathcal{M}_{\text{det}}h^3/\text{step}$	pilot substeps
\mathcal{M}_1 equation 8	Itô coefficient	localizes SDE cost; $\beta\mathcal{M}_1h^2/\text{step}$	kicks equation 9

Table 1: The audit interface. Inputs: checkpoint (D_θ, η_θ) , mesh $\{\sigma_n\}$, policy (clock, gauge, β , frozen object). Outputs: the four functionals above and the hypotheses equation 16—each an expectation of η -increments of the pretrained network.

a Hutchinson-type reading at $O(1)$ extra NFE per probe. Gaussian probes measure the Frobenius norm, $\mathbb{E}_z \|Az\|^2 = \|A\|_F^2$, whatever the symmetry of A ; the trace form $\frac{1}{D}\mathbb{E} \text{tr}(I - J_D)^2$ coincides with equation 8 iff J_D is symmetric: exact for a Tweedie denoiser, $J_D = \text{Cov}[X_0 | X]/\sigma^2$ PSD (equation 3), but not for a learned one. Definition 2 therefore takes the Frobenius form as primitive, the trace form being its exact-denoiser case.

Standing assumption (A): for $\sigma \in [\sigma_{\min}, \sigma_{\max}]$, $D(\cdot, \sigma) \in C^2(\mathbb{R}^D)$ with $\eta, D_\lambda \eta, I - J_D$, and the third-order Taylor remainders square-integrable along the flows considered; constants below depend on the data only through the displayed functionals. On the models of §4–5, (A) holds with every quantity closed-form.

In λ -time the marginal-preserving family (equation 4) reads $dX_\lambda = (1 + \beta)(D - X_\lambda) d\lambda + \sqrt{2\beta} \sigma_\lambda dW_\lambda$, with $\beta = 0$ the PF-ODE.

Theorem 1 (Local residual law). *Fix $\beta \geq 0$, let X solve the family on $[\lambda, \lambda + \tau]$ with marginals p_σ , and write $\Delta\eta = \eta(X_{\lambda+\tau}, \lambda + \tau) - \eta(X_\lambda, \lambda)$. Under (A):*

(i) (Deterministic law.) *For $\beta = 0$,*

$$\frac{1}{D} \mathbb{E} \|\Delta\eta\|^2 = \mathcal{M}_{\text{det}}(\lambda) \tau^2 + O(\tau^3). \quad (10)$$

(ii) (Stochastic law.) *For $\beta > 0$, the martingale part of $d\eta$ is $\sqrt{2\beta}(I - J_D) dW_\lambda$ —the injected noise’s σ and the σ^{-1} of $\nabla_x \eta = (I - J_D)/\sigma$ cancel, leaving no σ -weight—and*

$$\frac{1}{D} \mathbb{E} \|\Delta\eta\|^2 = 2\beta \mathcal{M}_1(\lambda) \tau + O(\tau^2), \quad (11)$$

the $O(\tau^2)$ coefficient reducing to \mathcal{M}_{det} at $\beta = 0$.

(iii) (Chart covariance.) *For a repackaged target $\zeta = c(\sigma_\lambda) \eta$ with $c \in C^1$ (Table 3), laws (i)–(ii) hold for ζ with coefficients*

$$\mathcal{M}_{\text{det}}^{(\zeta)}(\lambda) = \frac{1}{D} \mathbb{E} \|\dot{c}\eta + cD_\lambda \eta\|^2, \quad 2\beta c(\sigma_\lambda)^2 \mathcal{M}_1(\lambda), \quad \dot{c} = \frac{d}{d\lambda} c(\sigma_\lambda) = -\sigma c'(\sigma). \quad (12)$$

The exponents τ^2 and τ^1 are therefore invariant across every affine repackaging of Table 3; for the coefficients, the chart law above is proved for a rescaling $\zeta = c(\sigma)\eta$, and adding a D -part $b(\sigma)D$ only perturbs them at $O(\sigma)$ (its martingale is the σ -weighted $\sigma J_D \sqrt{2\beta} dW$). Given (A) and $m_1, \mathcal{M}_{\text{det}}, \mathcal{M}_1 = O(1)$, σ -uniform boundedness then holds iff c is bounded as $\sigma \rightarrow 0$. The bare score, $c(\sigma) = -\sigma^{-1}$, inflates both coefficients by σ^{-2} against $O(1)$ numerators; its integrated Itô budget becomes $\int_0^\Lambda 2\beta c^2 \mathcal{M}_1 d\lambda = \beta \mathcal{M}_1(\sigma_{\min}) \sigma_{\min}^{-2} (1 + o(1))$ (for \mathcal{M}_1 continuous and non-vanishing at the floor), concentrated in the final e -fold of scale, in place of the horizon-extensive $2\beta \overline{\mathcal{M}_1} \Lambda$ of the η -chart.

Proof. Itô’s formula in the chart η ; the one cancellation is stated in (ii). Appendix A. \square

Remark 2 (Exact law vs. operational audit). Theorem 1 is stated for the exact family: the expectations are over the true marginals p_σ and J_D is the exact Tweedie Jacobian. The runtime audit of §6 replaces these by pilot-probe distributions and logged trajectories of the *learned* field, so it estimates the discretization budget of the learned checkpoint (the first term of Proposition 1), not the true data-flow budget; the difference is the model error δ , which the audit does not measure.

Exponents are geometry; coefficients are the chart. The measured $p \approx 2 / p \approx 1$ of §6 survive any repackaging of Table 3; what the micro variable buys, and the audit requires, is the σ -uniform $O(1)$ coefficient: the estimate commuting with $\sigma_{\min} \rightarrow 0$ exactly as Definition 1 demands of the scheme. Part (iii) makes Table 3’s caption quantitative: a score target is usable only through a bounded repackaging, never audited bare.

Corollary 1 (Budgets and mesh laws). *Let the mesh be quasi-uniform with maximal step $h \leq 1$. (a) One step. On $[\lambda_n, \lambda_n + h_n]$,*

$$\frac{1}{D} \mathbb{E} \int_0^{h_n} \|\eta(\lambda_n + t) - \eta(\lambda_n)\|^2 dt = \begin{cases} \frac{1}{3} \mathcal{M}_{\det}(\lambda_n) h_n^3 + O(h_n^4), & \beta = 0, \\ \beta \mathcal{M}_1(\lambda_n) h_n^2 + O(h_n^3), & \beta > 0. \end{cases} \quad (13)$$

(b) Mesh sums. *Summing equation 13 over a mesh with $h = \Lambda/N$ (spectra evaluated on exact marginals; the numerical-path substitution costs $O(h)$, absorbed in the stated factors),*

$$\mathcal{E}_2^{\text{flow}}|_{\beta=0} = \frac{C_{\det}}{3} \frac{\Lambda^2}{N^2} (1+O(h)), \quad \mathcal{E}_2^{\text{flow}}|_{\beta>0} = \beta \overline{\mathcal{M}_1} \frac{\Lambda^2}{N} (1+O(h)), \quad (14)$$

with $C_{\det} := \int_0^\Lambda \mathcal{M}_{\det} d\lambda$ and $\overline{\mathcal{M}_1} := \Lambda^{-1} \int_0^\Lambda \mathcal{M}_1 d\lambda$. (c) Metric conversion. For $\beta > 0$, Girsanov converts the per-dimension budget to the per-dimension path divergence $\text{KL}_{\text{path}} := D^{-1} \text{KL}(P^h \| P)$, every σ -weight cancelling,

$$\text{KL}_{\text{path}} = \frac{(1+\beta)^2}{4\beta} \mathcal{E}_2^{\text{frozen}}, \quad \text{hence} \quad \text{KL}_{\text{path}} = \frac{(1+\beta)^2}{4} \overline{\mathcal{M}_1} \frac{\Lambda^2}{N} (1+O(h)); \quad (15)$$

at $\beta = 1$ and $\overline{\mathcal{M}_1} = (D-d)/D$ (rank-deficient data, §5) this recovers the Λ^2/N against Λ^2/N^2 separation as a corollary. For $\beta = 0$ the path measures are mutually singular and no path-KL exists; \mathcal{E}_2 is then the L^2 discretization functional of the learned flow, whose density \mathcal{M}_{\det} is the same scale-local budget that prices the W_2 theorems of §4–5, a surrogate with shared currency, not a bound.

On the calibration models the deterministic budget is $O(1)$ and explicit: $C_{\det} = d/(4D)$ on the rank-deficient Gaussian (exactly $\frac{1}{4}$ per data-carrying coordinate, cost density $u/(1+u)^3$, $u = \sigma^2/c_i$, peaking at $\sigma^2 = c_i/2$) and $\mathfrak{C} \approx 1.01$ on the mixture ($\int \mathcal{M}_{\det} d\lambda$; §5), matched asymptotics $\frac{1}{4} + \frac{3\pi}{16}$, the Gaussian core $\frac{1}{4}$ the same in both. The stochastic spectrum instead plateaus at $\overline{\mathcal{M}_1} = (D-d)/D$ over an $O(\Lambda)$ terminal portion: the deterministic budget is scale-local (a band around the data spectrum), the Itô budget scale-extensive: the mechanism behind the logarithm’s assignment in §5.

Design hypotheses. Given the local laws, classical equidistribution of the per-step budgets equation 13 over $\int n(\lambda) d\lambda = N$ steps prescribes local step densities

$$(H) \quad n_{\text{ODE}}(\lambda) \propto \mathcal{M}_{\det}(\lambda)^{1/3}, \quad n_{\text{SDE}}(\lambda) \propto \mathcal{M}_1(\lambda)^{1/2}. \quad (16)$$

We record equation 16 as falsifiable consequences of the audit, not as guaranteed samplers: a scalar ledger ignores coupling between coordinates, solver order, finite-step nonlinearity, and the geometry of perceptual metrics. A companion negative gate makes the boundary concrete: the ledger-optimal scalar-freeze schedule $c^*(\sigma) = 1 - m_1(\sigma)$ is not FID-optimal in a 2048-image CIFAR pilot (Appendix H). Accordingly we claim no better sampler than a tuned schedule.

The learned-field boundary. The audit sees only the checkpoint. Writing $\eta_\theta = \eta_\star + \delta$, with η_\star the exact residual of $\{p_\sigma\}$, separates what it can and cannot certify.

Proposition 1 (Audited term plus model term). *For $\beta > 0$, the per-dimension path divergence of the frozen- η_θ sampler P_θ^h against the exact reverse process P_\star obeys*

$$\text{KL}_{\text{path}}(P_\theta^h \| P_\star) \leq \frac{(1+\beta)^2}{2\beta} \left[\mathcal{E}_2^{\text{frozen}}(\eta_\theta) + \frac{1}{D} \mathbb{E} \int_0^\Lambda \|\delta(X_\lambda, \lambda)\|^2 d\lambda \right]. \quad (17)$$

The first term is the audited discretization budget of Definition 2 in its frozen-drift form $\mathcal{E}_2^{\text{frozen}}$, the KL-facing object (the predictive gates of §6 use $\mathcal{E}_2^{\text{flow}}$); the second is model error, and no functional of η_θ alone can bound it.

Proof. The Girsanov drift gap is $(1 + \beta)\sigma[(\eta_\theta\text{-frozen} - \eta_\theta) + \delta]$; Young’s inequality $\|a - b\|^2 \leq 2\|a\|^2 + 2\|b\|^2$ and equation 15. Appendix A. \square

The audit is thus scoped exactly: it certifies the discretization of the learned flow, uniformly in σ_{\min} , and is silent on δ , since measuring δ is what would require ground truth.

Relation to classical a posteriori estimation. The audit is a posteriori in the classical sense—residual-based, computed from the numerical solution—in the lineage of embedded ODE estimators (Hairer et al., 1993), finite-element residual indicators (Verfürth, 1996), and adaptive SDE solvers (Jolicoeur-Martineau et al., 2021). What is new is uniformity in the singular parameter: classical indicators’ constants degenerate exactly where sampling lives (score Lipschitz $\sim \sigma_{\min}^{-2}$), whereas every functional of Definition 2 carries $O(1)$ coefficients as $\sigma_{\min} \rightarrow 0$: asymptotic-preserving a posteriori estimation, calibrated by the closed-form constants of §4–5 (Appendix J). In contrast to schedule-optimization methods such as Align Your Steps (Sabour et al., 2024) and adaptive solvers (Jolicoeur-Martineau et al., 2021), which *choose* steps to minimize an error surrogate, the audit *estimates* and localizes discretization cost without prescribing a schedule; the negative gate (Appendix H) shows that ledger improvements need not improve FID.

The remainder calibrates these functionals on solvable models (§4–5) and measures them on a pre-trained checkpoint (§6), marking where the ledger certifies and where FID geometry departs.

4 CALIBRATION I: THE GAUSSIAN MODEL

The calibration of §3 uses solvable models with every audit functional closed-form and every sharp constant named. The first is the rank-deficient Gaussian, which calibrates by coordinate type. Normal coordinates ($c_i = 0$) carry the pure terminal layer and price the stability certificate E1, a clock barrier with two constants, the Lambert- W threshold $h_* = 1 + W(1/e)$ and the Wallis floor $1/\sqrt{\pi}$ (§4.1). Tangential coordinates ($c_i > 0$) carry the data and price the deterministic budget \mathcal{M}_{\det} , a one-sided covariance contraction with sharp constant $\frac{1}{4}$, integrating to $C_{\det} = d/(4D)$ (§4.2). Together they give the linear rung’s verdict: DDIM is first-order uniformly accurate in σ_{\min} , and the schedule is demoted to resolving the data’s spectral band.

Setup. Let $p_0 = \mathcal{N}(0, C)$ with spectrum $c_1 \geq \dots \geq c_d > 0 = c_{d+1} = \dots = c_D$ and data manifold $\mathcal{M} = \text{ran } C$. Then $p_\sigma = \mathcal{N}(0, C + \sigma^2 I)$, the exact denoiser is linear, $D(x, \sigma) = C(C + \sigma^2 I)^{-1}x$ (so $J_D = C(C + \sigma^2 I)^{-1}$ is symmetric with spectrum $c_i/(c_i + \sigma^2) \in [0, 1)$) and equation 1 diagonalizes with $\eta_i = \sigma x_i/(c_i + \sigma^2)$. The exact solution is $x_i(\sigma) = x_i(\sigma_{\max})\sqrt{(c_i + \sigma^2)/(c_i + \sigma_{\max}^2)}$; on normal coordinates ($c_i = 0$) this is the pure terminal layer $x_i(\sigma) \propto \sigma$, $\eta_i = x_i/\sigma$, while on tangential coordinates ($c_i > 0$) it is not a layer but a transition, completed around $\sigma^2 \approx c_i$. The model splits into two coordinate types, each with its own calibration.

Lemma 1 (Continuous residual law). *Along the exact flow $d\eta_i/d\sigma = c_i x_i/(c_i + \sigma^2)^2$, so η_i keeps the sign of x_i and $d|\eta_i|/d\sigma = c_i|x_i|/(c_i + \sigma^2)^2 \geq 0$. Hence normal coordinates conserve η_i exactly, and tangential coordinates satisfy $|\eta_i(\sigma)| = |x_i(\sigma_{\max})|\sigma/\sqrt{(c_i + \sigma^2)(c_i + \sigma_{\max}^2)}$, which decreases monotonically along sampling ($\sigma \downarrow$). In particular $\|\eta(\sigma)\|$ is non-increasing along sampling, uniformly in σ_{\min} .*

The exact flow thus passes the audit: the certificate equation 6 holds with equality on normal coordinates and strict decrease on tangential ones: the continuous law any discretization is read against.

One scheme, three forms. For a clock $\tau = \phi(\sigma)$, explicit Euler with a frozen denoiser is $x_{n+1} = x_n + \frac{\phi(\sigma_{n+1}) - \phi(\sigma_n)}{\phi'(\sigma_n)} \eta_n$. The following identity holds for any denoiser and exhibits DDIM as a fitted operator; it is the zeroth-order exponential-integrator step of Lu et al. (2022); Zhang & Chen (2022).

Proposition 2 (σ -clock Euler = DDIM). *For $\phi = \text{id}$ and any denoiser D ,*

$$x_{n+1} = x_n + (\sigma_{n+1} - \sigma_n) \eta_n = D_n + \sigma_{n+1} \eta_n = \frac{\sigma_{n+1}}{\sigma_n} x_n + \left(1 - \frac{\sigma_{n+1}}{\sigma_n}\right) D_n, \quad (18)$$

which is exactly the deterministic DDIM update (Song et al., 2020a): decompose into denoiser plus residual, then rescale the residual to the new noise level.

Proof. Immediate from $\eta_n = (x_n - D_n)/\sigma_n$; no linearity or Gaussianity is used. \square

4.1 THE CLOCK BARRIER

On a normal coordinate every clock’s Euler step is a linear update $x_{n+1} = (1 - \psi_\phi(h_n))x_n$ with $\psi_\phi(h) = [\phi(\sigma) - \phi(\sigma e^{-h})]/(\sigma\phi'(\sigma))$, giving $\psi_\sigma(h) = 1 - e^{-h}$, $\psi_\lambda(h) = h$, and $\psi_{\sigma^2}(h) = (1 - e^{-2h})/2$. Define the per-step *residual amplification* $A_\phi(h) = |\eta_{n+1}|/|\eta_n| = |1 - \psi_\phi(h)| e^h$ on the normal coordinate; the exact flow demands $A \equiv 1$ (Lemma 1).

Proposition 3 (Layer-exact clocks). *Euler-in- ϕ integrates the normal coordinate exactly on every mesh iff $\psi_\phi(h) = 1 - e^{-h}$ for all σ, h , iff ϕ is affine in σ . Thus the σ -clock is the unique layer-exact clock up to affine reparameterization.*

Proof. Exactness requires $\phi(\sigma) - \phi(\sigma e^{-h}) = \sigma\phi'(\sigma)(1 - e^{-h})$ for all h ; differentiating in h gives $\phi'(\sigma e^{-h}) = \phi'(\sigma)$, so ϕ' is constant. Euler is affine-covariant, so “up to affine” is best possible. \square

The three clocks separate sharply, with two named constants: the Lambert- W function (Corless et al., 1996) and the Wallis constant.

Theorem 2 (Normal-layer clock barrier). *On the normal coordinate $x'(\sigma) = x/\sigma$, $\eta = x/\sigma$:*

- (a) **σ -clock / DDIM.** $A_\sigma(h) \equiv 1$: *the step is layer-exact and conserves η (E1 equality) on every mesh, for every σ_{\min} .*
- (b) **λ -clock.** $A_\lambda(h) = |1 - h| e^h$. *The E1 nonexpansion $A_\lambda(h) \leq 1$ holds iff $h \leq h_\star = 1 + W(1/e) = 1.27846\dots$, equivalently $\sigma_{n+1}/\sigma_n \geq W(1/e) = 0.27846\dots$ (each step may shrink σ by at most $\approx 3.59\times$). Absolute stability holds up to $h \leq 2$; the window $(h_\star, 2]$ is stable but E1-expansive.*
- (c) **Heat-clock.** $A_{\text{heat}}(h) = \cosh h > 1$ for every $h > 0$: *there is no nontrivial E1-monotone step, so no fixed- N heat mesh is residual-AP as $\sigma_{\min} \rightarrow 0$. On the uniform heat mesh the normal standard deviation stagnates, $\text{std}_\perp(x_N) \rightarrow \sigma_{\max} \frac{(2N-1)!!}{(2N)!!} \sim \sigma_{\max}/\sqrt{\pi N}$, a σ_{\min} -independent floor with sharp Wallis constant $1/\sqrt{\pi}$.*

In words: the practitioners’ clock is the *only* exactly stable one (a); the log-SNR clock is safe only up to h_\star (b); and the uniform- σ^2 heat clock cannot resolve the layer (c), stalling a distance $\sigma_{\max}/\sqrt{\pi N}$ from the data whatever σ_{\min} is; so reaching $W_2 \leq \text{tol}$ costs $N \gtrsim \sigma_{\max}^2/(\pi \text{tol}^2)$, a quadratic price the σ -clock avoids. This calibrates E1: the certificate equation 6 has its equality case (the σ -clock), its sharp boundary (h_\star), and its failure floor (the Wallis constant $1/\sqrt{\pi}$), all closed-form, the three numbers a runtime reading of E1 is judged against.

Remark 3 (E1 is stability, not accuracy). The λ -clock with $h = 1$ sends the normal coordinate to zero in one step: $A_\lambda(1) = 0$, so E1 strictly decreases, yet the finite- σ solution is wrong. E1 rules out unresolved terminal-layer blow-up; it does not imply consistency. UA still requires the tangential accuracy analysis below (§4.2).

This is why EDM’s identity clock $\phi(\sigma) = \sigma$ (Karras et al., 2022) is special: the unique layer-exact clock up to affine change, obtained as a rigidity theorem rather than by design-space search.

The same layer-exactness question resolves cleanly for flow matching.

Proposition 4 (Flow-matching layer-exactness). *For a Gaussian-path sampler $X_t = \alpha_t X_0 + \sigma_t Z$, frozen-velocity Euler integrates a normal coordinate exactly on every mesh iff the noise schedule σ_t is affine in the sampler’s time t ; the affine gauge α_t does not affect the classification. The optimal-transport / rectified-flow schedule $\sigma_t = t$ satisfies this.*

The proof (Appendix B) is a one-line normal-coordinate check. So rectified flow ($\sigma_t = t$) is a second layer-exact scheme alongside the σ -clock/DDIM (a fitted-operator reason linear schedules sample well) and is the flow-matching counterpart of Proposition 3: both say the relevant noise level (VE σ for DDIM, interpolant σ_t for flow matching) must be affine in the stepping variable. Schedules with σ_t nonlinear in t inherit the λ - and heat-clock amplification of Theorem 2, and Theorem 3’s tangential covariance loss applies after the change of variables equation 5.

Layer-exactness, though, is only stability: by Remark 3 it says nothing about accuracy on the data-carrying tangential directions; the tangential covariance loss below governs those.

4.2 TANGENTIAL COVARIANCE LOSS AND UNIFORM ACCURACY

Theorem 2 settles the normal layer; the accuracy of DDIM is decided on the tangential ($c_i > 0$) coordinates, where the exact flow is not a pure layer. Here DDIM is not exact but its error is one-sided and sharply bounded.

Theorem 3 (Tangential covariance loss). *Under the σ -clock/DDIM step on the Gaussian model, a tangential coordinate with eigenvalue $c > 0$ contracts one-sidedly: its per-step numerical-to-exact standard-deviation ratio is $\rho_n = (c + \sigma_n \sigma_{n+1}) / \sqrt{(c + \sigma_n^2)(c + \sigma_{n+1}^2)} \leq 1$. If $\max_n h_n \leq h \leq 1$, the total contraction $\rho = \prod_n \rho_n$ obeys, uniformly in c and σ_{\min} ,*

$$0 \leq -\log \rho \leq \frac{h}{4} + O(h^2), \quad (19)$$

and the leading constant $1/4$ is sharp as $h \rightarrow 0$ (attained when the coordinate's transition lies strictly inside the range, $\sigma_{\min}^2 \ll c \ll \sigma_{\max}^2$).

The proof (Appendix C) localizes each coordinate's loss to a one-octave λ -window $|\log(\sigma^2/c_i)| \lesssim 1$ via a weighted midpoint quadrature in $y = \log(\sigma^2/c)$, so point-clustering cannot inflate the sum.

The theorem's constant has an integrated twin, the deterministic budget §3 states after Corollary 1.

Corollary 2 (Gaussian deterministic budget). *On the model the deterministic scale spectrum of equation 8 is closed-form: with $u_i = \sigma^2/c_i$,*

$$\mathbb{E}_{p_\sigma} |D_\lambda \eta_i|^2 = \frac{\sigma^2 c_i^2}{(c_i + \sigma^2)^3} = \frac{u_i}{(1 + u_i)^3}, \quad \mathcal{M}_{\det}(\sigma) = \frac{1}{D} \sum_{i: c_i > 0} \frac{u_i}{(1 + u_i)^3}, \quad (20)$$

normal coordinates contributing nothing. Each active coordinate's cost density in λ peaks at $\sigma^2 = c_i/2$ and integrates to exactly $\frac{1}{4}$:

$$C_{\det} = \int_0^\Lambda \mathcal{M}_{\det} d\lambda = \frac{1}{D} \sum_{i: c_i > 0} \frac{1}{2} \int_{\sigma_{\min}^2/c_i}^{\sigma_{\max}^2/c_i} \frac{du}{(1 + u)^3} = \frac{d}{4D} \left(1 + O\left(\frac{\sigma_{\min}^2}{c_d}\right) + O\left(\frac{c_1^2}{\sigma_{\max}^4}\right) \right), \quad (21)$$

independent of σ_{\min} .

Proof. Appendix I. □

Three readings follow (Appendix J): the theorem gives $h/4$ and the budget a per-coordinate $\frac{1}{4}$, one octave-local integral read a factor of h apart; the density peaks at $\sigma^2 = c_i/2$, so the deterministic ledger charges only the band $[\sqrt{c_d}, \sqrt{c_1}]$ a schedule must resolve; and under the inversion $u = 1/\sigma^2$ that same integral becomes the Gaussian core $\frac{1}{4}$ of the mixture budget $\frac{1}{4} + \frac{3\pi}{16}$ (Theorem 4, at $c = m^2$).

Combining tangential contraction with normal exactness gives the uniform-accuracy payoff.

Corollary 3 (DDIM is σ_{\min} -uniformly accurate on the Gaussian model). *On the λ -quasi-uniform mesh ($\max_n h_n \leq h \leq 1$), normal directions are exact and*

$$W_2(\text{Law}(x_N), p_{\sigma_{\min}}) \leq \left(\frac{h}{4} + O(h^2) \right) \sqrt{\sum_{i: c_i > 0} (c_i + \sigma_{\min}^2)} \xrightarrow{\sigma_{\min} \rightarrow 0} \left(\frac{h}{4} + O(h^2) \right) \sqrt{\text{tr } C}, \quad (22)$$

with constant independent of σ_{\min} . DDIM is thus first-order UA on rank-deficient Gaussian data.

Reading the bound at $\sigma_{\min} \rightarrow 0$ confirms AP-consistency: the error saturates at a finite, σ_{\min} -free value governed by the data spectrum, not by the terminal floor (Figure 1a). The step bound $\max_n h_n \leq h$ binds only on the data band $[\sqrt{c_d}, \sqrt{c_1}]$: on the *active-band mesh* (quasi-uniform down to $\sigma_a = h\sqrt{c_d}$, then a single step to σ_{\min}), each tangential coordinate is already contracted below the band ($u_i = \sigma_a^2/c_i \leq h^2$), so the terminal step adds only $\frac{1}{2} \log(1 + \sigma_a^2/c_i) \leq \sigma_a^2/2c_i \leq h^2/2$ per coordinate, from the identity $(c_i + \sigma_a \sigma_{\min})^2 + c_i(\sigma_a - \sigma_{\min})^2 = (c_i + \sigma_a^2)(c_i + \sigma_{\min}^2)$, absorbed in the $O(h^2)$. Hence $N = O((\log(c_1/c_d) + \log(1/h))/h)$ is σ_{\min} -free, and the accuracy, not just its constant, escapes $\log(1/\sigma_{\min})$.

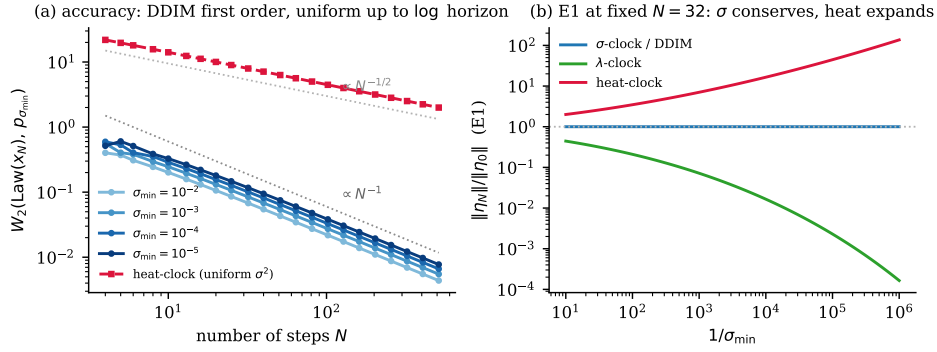


Figure 1: Uniform-in- σ_{\min} behaviour on the rank-deficient Gaussian, closed-form from Theorems 2–3. **(a)** Terminal W_2 vs. steps N (λ -uniform mesh): DDIM (σ -clock) is first order, its curves for $\sigma_{\min} \in \{10^{-2}, \dots, 10^{-5}\}$ nearly coincident (only σ_{\min} -dependence is $\Lambda = \log(\sigma_{\max}/\sigma_{\min})$ in $h = \Lambda/N$; Corollary 3), while the uniform- σ^2 heat-clock stagnates at the Wallis floor $\sigma_{\max}/\sqrt{\pi N}$ (Theorem 2c). **(b)** Residual amplification $\|\eta_N\|/\|\eta_0\|$ (E1, $N = 32$): the σ -clock conserves ($\equiv 1$), the heat-clock expands ($\cosh h$), the λ -clock drives to zero; E1 certifies stability, not accuracy (Remark 3).

Remark 4 (Oversmoothing, and a derived schedule). The one-sidedness $\rho \leq 1$ is the sharp, signed version of the folklore that low-NFE DDIM loses contrast: each data direction’s numerical standard deviation is at least $e^{-h/4}$ times the exact one. Because the loss weight concentrates on the band $\sigma \in [\sqrt{c_d}, \sqrt{c_1}]$, resolving it with $N = O(\log(c_1/c_d)/h)$ is all a schedule must do: the linear-model instance of “AP demotes the schedule to a second-order concern.”

This closes the Gaussian calibration. E1 is priced at its equality case (the σ -clock), its sharp boundary (h_*), and its failure floor (the Wallis constant); \mathcal{M}_{\det} integrates to $d/(4D)$, its mass confined to the data band; and DDIM is first-order UA with a σ_{\min} -free constant, the schedule demoted to resolving $[\sqrt{c_d}, \sqrt{c_1}]$. Two bills the model cannot present: linearity has no switching, and layer exactness says nothing about the Itô term a stochastic traversal pays. Section 5 prices both: the interface at a universal constant, the noise at the logarithm.

5 CALIBRATION II: INTERFACES AND STOCHASTICITY

The second calibration is the first nonlinearity: a two-point mixture, explicit enough to compute, yet carrying the obstruction the Gaussian lacks: posterior switching across an interface. *A symmetric interface does not charge a logarithm; noise does*: the interface destroys pointwise accuracy but charges the *deterministic* sampler no logarithm, while the logarithm lives instead in the Itô term of *stochastic* samplers, already for rank-deficient Gaussian data.

Setup. Take the symmetric mixture $p_0 = \frac{1}{2}\delta_{-m} + \frac{1}{2}\delta_{+m}$, $\Delta = 2m$; transverse directions decouple as Gaussian normal coordinates (Theorem 2a), so the problem is one-dimensional. Then

$$D(x, \sigma) = m \tanh \theta, \quad \theta = \frac{mx}{\sigma^2}, \quad s = \frac{m^2}{\sigma^2} = \frac{\Delta^2}{4\sigma^2}, \quad (23)$$

with $\text{Var}[x_0 | x] = m^2 \text{sech}^2 \theta$ and $D_x = s \text{sech}^2 \theta = \text{Var}[x_0 | x]/\sigma^2$ (the scalar entry of J_D). Here θ is the spatial inner coordinate and s the stiffness; $s = 1$ ($\sigma = \Delta/2$) is the classical unimodal-to-bimodal threshold. In λ -time the inner variable obeys $\dot{\theta} = \theta + s \tanh \theta$ and the normalized residual obeys the material-derivative identity ($D_\lambda = d/d\lambda$ along the flow $dX/d\lambda = D - X$)

$$D_\lambda \eta = \eta D_x + D_\sigma = -\frac{\text{Var}[x_0 | x]}{m\sigma} \dot{\theta}, \quad (24)$$

i.e. the local error density factors into an inner velocity and a posterior-variance weight.

5.1 GEOMETRY OF THE SWITCHING LAYER

Proposition 5 (The interface is triple-thin). *The switching layer is the expansion set $\mathcal{L}_\sigma = \{x : D_x > 1\} = \{\text{Var}[x_0 | x] > \sigma^2\}$, the complement of the Brascamp–Lieb log-concave contraction regime (Brascamp & Lieb, 1976). In the symmetric model $D_x = s \operatorname{sech}^2 \theta \geq 1$ iff $\cosh \theta \leq \sqrt{s}$, so for $s \gg 1$ the layer has physical half-width*

$$w(\sigma) = \frac{\sigma^2}{2m} \log(4m^2/\sigma^2) (1 + o(1)) = \frac{\sigma^2}{\Delta} \log \frac{\Delta^2}{\sigma^2} (1 + o(1)), \quad (25)$$

thinner than the normal layer by one power of σ . It is small in three senses at once: spatial width $O(\sigma^2/\Delta)$, probability mass $p_\sigma(\mathcal{L}_\sigma) \asymp \frac{\sigma}{\Delta} \log \frac{\Delta^2}{\sigma^2} e^{-\Delta^2/8\sigma^2}$ (exponentially small), and λ -residence $O(1/s)$. Yet the pointwise singularity is genuine: $\sup_x |D_\lambda \eta| \asymp s^{3/2}$ (Appendix D), and the limiting flow map $T(x) = m \operatorname{sign}(x)$ is discontinuous; so pointwise UA is impossible.

This is a caustic of singular-perturbation theory (Jin, 2022): smooth data, discontinuous limit map. The question is whether the blow-up carries enough mass to matter distributionally.

5.2 DETERMINISTIC SAMPLERS HAVE NO INTERFACE LOGARITHM

Theorem 4 (Deterministic budget is a universal constant). *The scale spectrum equation 8 of the mixture, here one-dimensional, $\mathcal{M}_{\text{det}}(\sigma) = \mathbb{E}_{p_\sigma} |D_\lambda \eta|^2$, depends by dimensional analysis only on s , and*

$$\mathcal{M}_{\text{det}}(s) = \begin{cases} s^2(1 + O(s)), & s \ll 1, \\ \frac{\sqrt{\pi/2}}{8} s^{5/2} e^{-s/2} (1 + O(s^{-1})), & s \gg 1. \end{cases} \quad (26)$$

Since $d\lambda = ds/2s$, the total budget $\mathfrak{C} = \int \mathcal{M}_{\text{det}} d\lambda$ is a universal constant, independent of m , σ_{\max} , and σ_{\min} , with matched-asymptotics estimate $\frac{1}{4}$ (Gaussian core, $s \ll 1$) + $\frac{3\pi}{16}$ (interface tail, $s \gg 1$) ≈ 0.84 ; direct quadrature gives $\mathfrak{C} \approx 1.01$.³ Consequently, deterministic DDIM-type samplers are first-order W_2 -UA on the mixture with constant independent of σ_{\min} and no $\log(1/\sigma_{\min})$ factor.

The Gaussian core is Corollary 2’s per-coordinate integral read at $c = m^2$ (the inversion $u = 1/s$ recorded there) so the mixture’s new expense is the tail alone: $\frac{3\pi}{16}$, the interface’s deterministic price (the remaining ≈ 0.17 of \mathfrak{C} sits in the $s = O(1)$ crossover, covered by neither asymptote). Two one-dimensional facts turn the finite budget into UA (Appendix D): DDIM is order-preserving ($dx_{n+1}/dx_n = e^{-h} + (1 - e^{-h})D_x > 0$ since $D_x \geq 0$), so $W_2^2 = \|T_{\text{num}} - T_{\text{exact}}\|_{L^2(p_{\sigma_{\max}})}^2$ with no coupling loss; and, by symmetry, $D(0, \sigma) = 0$ is a common fixed point, so both flows commit to the same basin, with no misclassification channel. The whole error is intra-basin plus the exponentially small layer, both absorbed by \mathfrak{C} . Symmetry is essential: an *asymmetric* mixture drifts the fixed point, so the flows can split between basins and the deterministic W_2 rate drops to $h^{1/2}$ when a commitment integral $\kappa \neq 0$ (Appendix E, sign open).

Remark 5 (Origin of a data-side logarithm). Theorem 4 refutes, for a single *symmetric* switching interface, the conjecture that it forces a $\log(1/\sigma_{\min})$ loss: a logarithm can only enter the *deterministic budget* from the data. If the data carry a hierarchy of separation scales down to σ_{\min} (a multiscale mixture), each active scale contributes an $O(1)$ budget over $O(\log(1/\sigma_{\min}))$ scales—so the logarithm is a property of scale-rich data, not of a single interface or the discretization.

5.3 THE LOGARITHMIC BARRIER BELONGS TO STOCHASTIC SAMPLERS

The deterministic budget must be corrected for the reverse SDE equation 4, but the correction is already priced. Theorem 1(ii) identified the martingale part of $d\eta$ as $\sqrt{2\beta} (I - J_D) dW_\lambda$, absent from the ODE, and Corollary 1 converted its quadratic variation into the per-step and mesh budgets equation 13, equation 14 and, via Girsanov, into path-KL equation 15. What remains open is the coefficient’s *extent*: \mathcal{M}_{det} closed in a band (Corollary 2); the separation of samplers turns on whether \mathcal{M}_1 is instead horizon-extensive: $O(1)$ over an $O(\Lambda)$ portion of scales. On the models it is, in closed form, and the logarithm follows by specialization of Theorem 1(ii).

³The budget density $\propto s^{5/2} e^{-s/2}$ peaks at $s_* = 5$ ($\sigma_* = \Delta/(2\sqrt{5}) \approx 0.224\Delta$): a mode pair of separation Δ demands the most resolution near that noise scale.

Corollary 4 (Stochastic Itô barrier). *Specializing Theorem 1(ii) and Corollary 1 to the models: on the rank-deficient Gaussian, $I - J_D$ has spectrum $\sigma^2/(c_i + \sigma^2)$, so with $u_i = \sigma^2/c_i$*

$$\mathcal{M}_1(\sigma) = \frac{1}{D} \left[(D-d) + \sum_{i: c_i > 0} \left(\frac{u_i}{1+u_i} \right)^2 \right] \xrightarrow{\sigma^2 \ll c_d} \frac{D-d}{D}, \quad (27)$$

an $O(1)$ plateau (≈ 1 for $d \ll D$; tending to 1 on a committed mixture direction, where $D_x \rightarrow 0$) over an $O(\Lambda)$ terminal portion, and the plateau is horizon-extensive: $\int_0^\Lambda \mathcal{M}_1 d\lambda = \frac{D-d}{D} \Lambda + O(1)$, the $O(1)$ independent of σ_{\min} . Hence, by the mesh law equation 14 and the Girsanov conversion equation 15, on the uniform λ -mesh with N steps at $\beta = 1$,

$$\text{KL}_{\text{disc}}^{\text{SDE}} \approx \frac{D-d}{D} \frac{\Lambda^2}{N}, \quad \text{versus} \quad E_2^{\text{ODE}} = O(\Lambda^2/N^2) \quad (28)$$

—the ODE carries no path-KL at $\beta = 0$ (Corollary 1(c)), so its residual budget E_2 is the shared-currency surrogate. The logarithmic horizon dependence of SDE sampling is thus intrinsic to the Itô term and present already for rank-deficient Gaussian data; it is not caused by the interface.

Proof. Appendix I. □

This separates ODE from SDE at the mechanism level, and it is the law behind the measured budget separation of §6: fitted slopes -1.991 against -0.977 (Figure 3a); it sharpens the upper bounds of Chen et al. (2022); Benton et al. (2024), which exhibit a logarithmic-in- $1/\sigma_{\min}$ cost but do not separate the two samplers.⁴ Against Corollary 2 the contrast is now formula-level: the deterministic density $u/(1+u)^3$ closes in a band— $\frac{1}{4}$ per coordinate—while the Itô spectrum equation 27 carries a σ -independent 1 on every normal coordinate, a charge per e -fold of scale: the scale-local/scale-extensive split of Corollary 1. Since \mathcal{M}_1 is a quadratic variation of η , a frozen- D update instead pays the complement $\frac{1}{D} \mathbb{E} \|J_D\|_F^2$. Once the posterior spectrum is anisotropic, cancelling both leading bills needs local Jacobian information—a Rosenbrock-type freeze (Appendix E); scalar preconditioning cannot.

6 THE PREDICTIVE AUDIT: CHECKPOINT EVIDENCE

On the official EDM CIFAR-10 unconditional VP checkpoint (Karras et al., 2022) ($\sigma \in [0.002, 80]$) the audit of §3 is read twice. Descriptively, from completed-step and injection-local increments of η : the exponents and coefficients of Theorem 1 (Figure 2). Predictively: spectra measured *once*, from 256 pilot states, forecast held-out residual budgets across step count, mesh schedule, and noise level β , against pre-specified gates with no per-configuration refitting (Figure 3, Table 2). The evidence is ordered by what each reading can and cannot show.

Exponents versus coefficients. The mesh laws equation 14 integrate the local exponents τ^2/τ^1 into N -scalings, and the checkpoint obeys them: on the λ -uniform mesh the deterministic budget falls at fitted slope -1.991 and the $\beta = 1$ flow budget at -0.977 ($N \geq 32$; Figure 3a)—the $p \approx 2/p \approx 1$ geometry of Theorem 1, invariant under every repackaging of Table 3 by part (iii). Alone, the exponents are cheap: any Itô process through a Lipschitz map has $O(\tau)$ quadratic variation and any smooth flow has $O(\tau^2)$ increments, so $p \approx 1$ certifies regularity and $p \approx 2$ smoothness, not the residual law. The law’s content is its *coefficients* ($2\beta\mathcal{M}_1$, with \mathcal{M}_1 the Frobenius mass of $I - J_D$), checkable against an object measured with no dynamics at all.

The control: the same- σ kick. The completed step cannot carry that check: deterministic and churned full-step increments nearly overlap (Figure 2a), mixing drift, injection, and denoising. The clean contact is the injection-local jump read against the same- σ kick equation 9, a perturbation at *fixed* σ , a static Jacobian reading blind to the sampler. If law (ii) is right, the dynamical jump coefficient must equal the static kick mass, scale by scale and churn strength by churn strength. It does. The two-moment inversion equation 29 (Appendix F) separates the churn jump’s deterministic dilation from its stochastic injection and, at full EDM strength ($\gamma = \sqrt{2}-1$, $S_{\text{noise}} = 1.003$), predicts

⁴Not in tension with Albergo et al. (2025)’s stricter likelihood control for deterministic dynamics, a global smoothness statement, versus our horizon-extensive Itô functional at the singular endpoint.

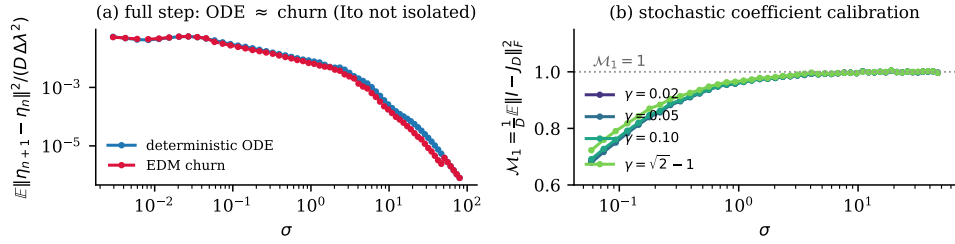


Figure 2: Scale spectrum on the pretrained EDM CIFAR-10 checkpoint (Karras et al., 2022) (256/128 seeds, 64 steps). **(a)** The full-step $\mathbb{E}\|\eta_{n+1} - \eta_n\|^2 / (D \Delta \lambda^2)$ for ODE and EDM churn nearly overlap: the completed step does not isolate the Itô term. **(b)** The injection-local churn jump, inverted via equation 29, reads $\mathcal{M}_1 = \frac{1}{D} \mathbb{E} \|I - J_D\|_F^2 = 1.00 \pm 0.01$ across the high/mid- σ plateau for $\gamma \in \{0.02, 0.05, 0.10, \sqrt{2} - 1\}$, a zero-parameter calibration of the functional of Corollary 4, drooping below 1 only as $\sigma \rightarrow 0$.

transfer axis	pre-specified gate	held-out outcome
step count ($N \in \{16, \dots, 256\}$)	ODE slope -2 ± 0.1 ; flow -1 ± 0.05 err $\leq 15\%$ ($N \geq 32$), $\leq 30\%$ ($N=16$)	-1.991 ; -0.977 $\leq 2.1\%$ ode, $\leq 5.3\%$ flow; 16.7%
schedule ($N=64$)	ranking kept; err $\leq 20\%$	exact, both β ; 2.7%/9.4%
noise ($\beta \in [\frac{1}{4}, 2]$)	linear in β : $R^2 \geq 0.99$, slope $\leq 10\%$	$R^2=0.99991$, slope -2.0% ($N=128$)

Table 2: Pre-specified transfer gates and held-out outcomes. Stage-0 spectra were fixed before the held-out runs; predictions use no per-configuration refitting. The noise transfer’s secondary case ($N = 64$) also passes the primary gate ($R^2 = 0.99969$, slope -6.0%).

1.699 against an observed 1.69–1.71 with no fitted parameter; an independent EM/ancestral probe agrees. This equality—a same-time derivative reading matching a dynamical jump, across four churn strengths and the σ -plateau—is what elevates $p \approx 1$ from Lipschitz-trivial to the specific martingale $\sqrt{2\beta} (I - J_D) dW_\lambda$ of Theorem 1(ii), cancellation included: no σ -weight survives in the measured coefficient across the plateau’s decades of scale.

The plateau coefficient. The plateau value itself, $\mathcal{M}_1 = 1.00 \pm 0.01$ (Figure 2b), is then a consistency number, not a headline: a CIFAR PCA Gaussian surrogate predicts it at $(D - d)/D \approx 1$ and leaves a positive low- σ residual—the droop as $\sigma \rightarrow 0$ is the non-Gaussian/interface discovery zone of §5, where a rank-deficient Gaussian surrogate must fail. Throughout, \mathcal{M}_1 is the Frobenius kick mass of Definition 2 (Remark 1); the trace form is its exact-denoiser special case.

The audit is predictive. The audit’s claim is not that the checkpoint obeys the law where it was measured, but that spectra measured once predict budgets not yet measured. Stage 0 fixes $\mathcal{M}_1(\sigma)$ (same- σ kicks) and $\mathcal{M}_{\text{det}}(\sigma)$ (centered differences of η along the flow) on a 40-point λ -grid from 256 forward-noised training states; every subsequent budget uses held-out seeds disjoint from the pilot, and every gate was fixed before the runs (Table 2; protocol in Appendix G). *Step count* (Figure 3a): predicted magnitudes match to $\leq 2.1\%$ (ODE) and $\leq 5.3\%$ (flow) for $N \geq 32$; the flow point at the coarsest mesh, $N = 16$, errs 16.7%, inside its pre-specified 30% gate. *Schedule* (Figure 3b, $N = 64$): re-quadrature of the same spectra over the λ and Karras $\rho \in \{3, 5, 7, 9\}$ meshes (the per-step laws equation 13 summed over each candidate mesh) reproduces the budget ordering exactly for both noise levels and the magnitudes to 2.7% (ODE) and 9.4% (flow); for $\beta = 1$ the two best schedules are statistically tied ($\rho = 9$: 1.3306 ± 0.0095 ; λ : 1.3320 ± 0.0065), so the audit’s claim is the ordering and the large gaps, with no winner among the tied pair. *Noise* (Figure 3c): the flow budget is linear in the noise level β , $\mathcal{E}_2^{\text{flow}}(\beta) = a + b\beta$ with $R^2 = 0.99991$ and slope within 2% of the pilot prediction at the primary $N = 128$, no per- β refit; the secondary $N = 64$ passes the same gate. Primary stochastic evidence throughout is the dense-substep budget along the true reverse dynamics equation 4, written $\mathcal{E}_2^{\text{flow}}$; the frozen-drift companion $\mathcal{E}_2^{\text{frozen}}$ (the object Girsanov

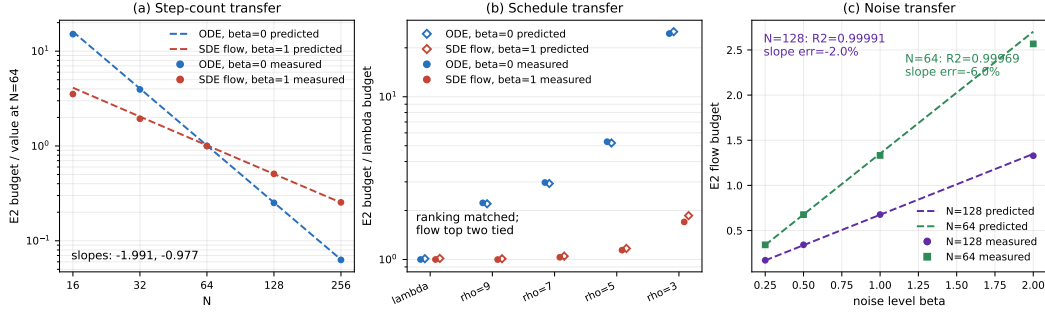


Figure 3: Predictive a posteriori audit on the pretrained EDM CIFAR-10 checkpoint. Pilot spectra measured once from 256 forward-noised states predict held-out budgets (disjoint seeds; pre-specified gates, Table 2), no refit. **(a)** Step-count transfer (λ -uniform): deterministic budget $\sim N^{-2}$, stochastic flow $\sim N^{-1}$ (slopes $-1.991, -0.977, N \geq 32$), the integrated exponents of Theorem 1; predictions match to $\leq 5.3\%$. **(b)** Schedule transfer ($N = 64$): re-quadrature over λ and Karras $\rho \in \{3, 5, 7, 9\}$ predicts the ordering exactly and magnitudes to $\leq 9.4\%$; at $\beta = 1$ the two best ($\rho = 9, \lambda$) tie. **(c)** Noise transfer: flow budget linear in β , $R^2 > 0.999$, slope within 2% of the pilot ($N = 128$), no per- β refit.

converts to path-KL in equation 15) exceeds it by $+87\%$ at $N = 16$ and $+1.1\%$ at $N = 256$, vanishing as the mesh refines, and is never used as a mesh-law gate (Appendix G).

Robustness across preconditioning. The deterministic \mathcal{M}_{det} predictor is a coherent τ^2 expansion and therefore requires local directional smoothness of $D_\lambda \eta$; the stochastic \mathcal{M}_1 predictor, by contrast, measures a quadratic variation and is direction-agnostic, which makes the stochastic leg the more robust transfer test. Running it on a second CIFAR-10 EDM checkpoint with VE/NCSN++ preconditioning, the same pilot \mathcal{M}_1 spectrum predicted held-out stochastic flow budgets across step count with relative error $+6.1\%$, $+2.4\%$, -0.03% at $N = 32, 64, 128$ (no per-configuration refit), so the Itô leg is not an artifact of the single VP checkpoint. We report this second checkpoint as a stochastic-robustness check only, not a full deterministic replication.

The boundary. What the campaign certifies is exactly the first term of Proposition 1: checkpoint-internal discretization budgets, predicted across held-out numerical configurations at the checkpoint’s fixed floor $\sigma_{\min} = 0.002$ (the audit’s σ_{\min} -uniformity is the theory’s claim, §4–5, not the single-floor campaign’s). It is silent on the model term δ , on other checkpoints, and on perceptual quality. None of the above claims a better sampler, a better schedule for image quality, or an FID improvement: the companion negative gate (the ledger-optimal scalar schedule c^* is not FID-optimal, Appendix H) remains the boundary the audit is honest about.

7 CONCLUSION

Treating the terminal noise floor σ_{\min} as a singular-perturbation parameter turns sampler design into asymptotic-preserving analysis and yields four results: a rigidity theorem (on the pure layer, the σ -clock/DDIM step and rectified flow are the unique layer-exact frozen-field Euler discretizations, up to affine reparameterization); a clean assignment of the logarithmic sampling cost (absent from the deterministic samplers on the calibrated models, including a symmetric posterior-switching interface, and intrinsic to the Itô term of stochastic ones: path-KL $\sim \Lambda^2/N$ against the ODE’s $O(\Lambda^2/N^2)$ budget); two runtime certificates, E1 stability and the E2 budget with its spectra $(\mathcal{M}_{\text{det}}, \mathcal{M}_1)$, all with σ_{\min} -uniform coefficients read from checkpoint evaluations on probe states; and a pre-specified predictive campaign in which spectra measured once on the EDM CIFAR-10 checkpoint forecast held-out residual budgets across step count, schedule, and noise level with no per-configuration refitting. The audit is scoped exactly: it certifies the discretization of the learned flow and is silent on model error and perceptual quality (Proposition 1). Three questions remain open: the sign of the commitment integral κ for asymmetric mixtures (Appendix E); a Rosenbrock-

exponential step that removes the horizon logarithm from stochastic sampling; and whether scale-rich data is where a deterministic logarithm returns.

REPRODUCIBILITY STATEMENT

All model problems (rank-deficient Gaussian, two-point mixture) are analytic and proved in the appendix. The CIFAR-10 probe uses the public EDM checkpoint and code of Karras et al. (2022) (`edm-cifar10-32x32-uncond-vp.pkl`; the second-checkpoint robustness check of §6 uses `edm-cifar10-32x32-uncond-ve.pkl`); the sampler step formulas and two-moment inversion are equation 18 and equation 29. The predictive audit (Appendix G) fixes its Stage-0 spectra on 256 forward-noised states and evaluates held-out budgets on the disjoint seeds 1000–1127; its per-configuration predictions and measurements ship as `predictions.csv` (33 rows) with the figures and logs, the refined $O(h)$ -corrected sums plotted in Figure 3. The diagnostic spectra of Figure 2 (pilot and churn runs, 256/128 seeds) and the predictive campaign of Figure 3 are separate runs; full per-configuration `.npz` archives are produced by the campaign script, and the released mirror keeps `predictions.csv`, the figures, and logs.

REFERENCES

- Michael Albergo, Nicholas M Boffi, and Eric Vanden-Eijnden. Stochastic interpolants: A unifying framework for flows and diffusions. *Journal of Machine Learning Research*, 26(209):1–80, 2025.
- Brian DO Anderson. Reverse-time diffusion equation models. *Stochastic Processes and their Applications*, 12(3):313–326, 1982.
- Joe Benton, Valentin De Bortoli, Arnaud Doucet, and George Deligiannidis. Nearly d -linear convergence bounds for diffusion models via stochastic localization. In *International Conference on Learning Representations*, volume 2024, pp. 36916–36936, 2024.
- Herm Jan Brascamp and Elliott H Lieb. On extensions of the brunn-minkowski and prékopa-leindler theorems, including inequalities for log concave functions, and with an application to the diffusion equation. *Journal of functional analysis*, 22(4):366–389, 1976.
- Sitan Chen, Sinho Chewi, Jerry Li, Yuanzhi Li, Adil Salim, and Anru R Zhang. Sampling is as easy as learning the score: theory for diffusion models with minimal data assumptions. *arXiv preprint arXiv:2209.11215*, 2022.
- Robert M Corless, Gaston H Gonnet, David EG Hare, David J Jeffrey, and Donald E Knuth. On the lambert w function. *Advances in Computational mathematics*, 5(1):329–359, 1996.
- Valentin De Bortoli. Convergence of denoising diffusion models under the manifold hypothesis. *arXiv preprint arXiv:2208.05314*, 2022.
- Bradley Efron. Tweedie’s formula and selection bias. *Journal of the American Statistical Association*, 106(496):1602–1614, 2011.
- Ernst Hairer, Gerhard Wanner, and Syvert P Nørsett. *Solving ordinary differential equations I: Nonstiff problems*. Springer, 1993.
- Shi Jin. Asymptotic-preserving schemes for multiscale physical problems. *Acta Numerica*, 31: 415–489, 2022.
- Alexia Jolicœur-Martineau, Ke Li, Rémi Piché-Taillefer, Tal Kachman, and Ioannis Mitliagkas. Gotta go fast when generating data with score-based models. *arXiv preprint arXiv:2105.14080*, 2021.
- Tero Karras, Miika Aittala, Timo Aila, and Samuli Laine. Elucidating the design space of diffusion-based generative models. *Advances in neural information processing systems*, 35:26565–26577, 2022.
- Yaron Lipman, Ricky TQ Chen, Heli Ben-Hamu, Maximilian Nickel, and Matt Le. Flow matching for generative modeling. *arXiv preprint arXiv:2210.02747*, 2022.

Xingchao Liu, Chengyue Gong, and Qiang Liu. Flow straight and fast: Learning to generate and transfer data with rectified flow. *arXiv preprint arXiv:2209.03003*, 2022.

Cheng Lu, Yuhao Zhou, Fan Bao, Jianfei Chen, Chongxuan Li, and Jun Zhu. Dpm-solver: A fast ode solver for diffusion probabilistic model sampling in around 10 steps. *Advances in neural information processing systems*, 35:5775–5787, 2022.

Herbert E Robbins. An empirical bayes approach to statistics. In *Breakthroughs in Statistics: Foundations and basic theory*, pp. 388–394. Springer, 1992.

Hans-Görg Roos, Martin Stynes, and Lutz Tobiska. *Robust numerical methods for singularly perturbed differential equations: convection-diffusion-reaction and flow problems*. Springer, 2008.

Amirmojtaba Sabour, Sanja Fidler, and Karsten Kreis. Align your steps: Optimizing sampling schedules in diffusion models. *arXiv preprint arXiv:2404.14507*, 2024.

Jiaming Song, Chenlin Meng, and Stefano Ermon. Denoising diffusion implicit models. *arXiv preprint arXiv:2010.02502*, 2020a.

Yang Song, Jascha Sohl-Dickstein, Diederik P Kingma, Abhishek Kumar, Stefano Ermon, and Ben Poole. Score-based generative modeling through stochastic differential equations. *arXiv preprint arXiv:2011.13456*, 2020b.

Rüdiger Verfürth. *A review of a posteriori error estimation and adaptive mesh-refinement techniques*. Wiley–Teubner, 1996.

Qinsheng Zhang and Yongxin Chen. Fast sampling of diffusion models with exponential integrator. *arXiv preprint arXiv:2204.13902*, 2022.

A PROOF OF THEOREM 1 (LOCAL RESIDUAL LAW)

Write $\eta = \eta(X_\lambda, \lambda)$ along the family $dX_\lambda = (1 + \beta)(D - X) d\lambda + \sqrt{2\beta} \sigma dW_\lambda$.

(i) Deterministic law. For $\beta = 0$ the flow is smooth and $\Delta\eta = D_\lambda\eta\tau + \frac{1}{2}D_\lambda^2\eta\tau^2 + O(\tau^3)$, so $\frac{1}{D}\mathbb{E}\|\Delta\eta\|^2 = \frac{1}{D}\mathbb{E}\|D_\lambda\eta\|^2\tau^2 + O(\tau^3) = \mathcal{M}_{\det}(\lambda)\tau^2 + O(\tau^3)$ by (A).

(ii) Stochastic law and the cancellation. Since $\eta = (X - D)/\sigma$ and $\nabla_x D = J_D$, Itô’s formula gives $d\eta = \mathcal{L}_\beta\eta d\lambda + \frac{1}{\sigma}(I - J_D) dX^{\text{mart}}$, where the generator \mathcal{L}_β collects the $(1 + \beta)(D - X)$ drift and the Itô correction and reduces to $D_\lambda\eta$ at $\beta = 0$; the martingale part of dX is $\sqrt{2\beta}\sigma dW$, so $d\eta^{\text{mart}} = \frac{1}{\sigma}(I - J_D)\sqrt{2\beta}\sigma dW = \sqrt{2\beta}(I - J_D) dW$: the σ of the injection and the σ^{-1} of $\nabla_x\eta$ cancel. The quadratic variation over $[\lambda, \lambda + \tau]$ is $2\beta(I - J_D)(I - J_D)^\top\tau + O(\tau^2)$, whose normalized trace is $\frac{1}{D}\mathbb{E}\|\Delta\eta\|^2 = 2\beta\frac{1}{D}\mathbb{E}\|I - J_D\|_F^2\tau + O(\tau^2) = 2\beta\mathcal{M}_1(\lambda)\tau + O(\tau^2)$; the $O(\tau^2)$ term carries the drift $\mathcal{L}_\beta\eta$, equal to $\mathcal{M}_{\det}\tau^2$ at $\beta = 0$ (where $\mathcal{L}_0\eta = D_\lambda\eta$).

(iii) Chart covariance. For $\zeta = c(\sigma_\lambda)\eta$, $D_\lambda\zeta = \dot{c}\eta + cD_\lambda\eta$ with $\dot{c} = -\sigma c'(\sigma)$, while the martingale part of $d\zeta$ is $c d\eta^{\text{mart}} = c\sqrt{2\beta}(I - J_D)dW$, giving the coefficients equation 12; the $\dot{c}\eta$ term is drift and enters the stochastic law at $O(\tau^2)$ only. For $c = -\sigma^{-1}$ (the bare score) the stochastic coefficient is $2\beta\mathcal{M}_1/\sigma^2$; since $d\lambda = -d\sigma/\sigma$, $\int_0^\lambda 2\beta c^2\mathcal{M}_1 d\lambda = 2\beta \int_{\sigma_{\min}}^{\sigma_{\max}} \mathcal{M}_1 \sigma^{-3} d\sigma = \beta\mathcal{M}_1(\sigma_{\min})\sigma_{\min}^{-2}(1 + o(1))$, endpoint-dominated.

Proposition 1. The frozen- η_θ sampler and the exact reverse process share the diffusion $\sqrt{2\beta}\sigma$; their drift gap is $(1 + \beta)\sigma[(\eta_\theta^{\text{frozen}} - \eta_\theta) + \delta]$. Girsanov equation 15 and $\|a - b\|^2 \leq 2\|a\|^2 + 2\|b\|^2$ give equation 17, all expectations under P_θ^h . \square

B PROOF OF THEOREM 2 (CLOCK BARRIER)

Work on a single normal coordinate ($c = 0$), where the exact flow is $x'(\sigma) = x/\sigma$, hence $x(\sigma) = x(\sigma_{\max})\sigma/\sigma_{\max}$ and $\eta = x/\sigma$ is constant. One frozen- η Euler step in the clock $\tau = \phi(\sigma)$ multiplies the coordinate by $1 - \psi_\phi(h)$, $\psi_\phi(h) = [\phi(\sigma) - \phi(\sigma e^{-h})]/(\sigma\phi'(\sigma))$, $h = \log(\sigma_n/\sigma_{n+1})$; since $\eta = x/\sigma$ and $\sigma_{n+1} = \sigma_n e^{-h}$, the residual amplification is $A_\phi(h) = |1 - \psi_\phi(h)| e^h$, and exactness means $A_\phi \equiv 1$.

(a) σ -clock. $\psi_\sigma(h) = 1 - e^{-h}$, so $A_\sigma(h) = e^{-h}e^h = 1$ for every h : layer-exact, with $\eta_{n+1} = \eta_n$ (E1 equality) on every mesh, uniformly in σ_{\min} .

(b) λ -clock. $\psi_\lambda(h) = h$, so $A_\lambda(h) = |1 - h|e^h$. On $[0, 1]$ it decreases from 1 to 0; on $[1, \infty)$, $A_\lambda(h) = (h - 1)e^h$ increases from 0 and crosses 1 at the unique root of $(h - 1)e^h = 1$. Writing $h = 1 + u$ gives $ue^{1+u} = 1$, i.e. $ue^u = e^{-1}$, whose solution is $u = W(1/e)$ (Corless et al., 1996); hence $h_\star = 1 + W(1/e) = 1.27846\dots$. From $ue^u = e^{-1}$ we get $e^{-u} = ue$, so $e^{-h_\star} = e^{-1}e^{-u} = e^{-1} \cdot ue = u = W(1/e) = 0.27846\dots$; thus $A_\lambda(h) \leq 1 \iff h \leq h_\star \iff \sigma_{n+1}/\sigma_n \geq W(1/e)$. Absolute stability of the x -iteration is $|1 - h| \leq 1$, i.e. $h \leq 2$; on $(h_\star, 2]$ the coordinate stays bounded while η grows by $A_\lambda(h) > 1$ per step. On the uniform λ -mesh $h = \Lambda/N$,

$$\frac{\|\eta_N\|}{\|\eta_0\|} = A_\lambda(h)^N = \left(|1 - \frac{\Lambda}{N}| e^{\Lambda/N}\right)^N = \left|1 - \frac{\Lambda}{N}\right|^N \frac{\sigma_{\max}}{\sigma_{\min}} \xrightarrow{\sigma_{\min} \rightarrow 0} \infty,$$

so E1 fails at rate σ_{\min}^{-1} up to a polylogarithmic factor for any fixed N .

(c) *Heat-clock*. $\phi(\sigma) = \sigma^2$ gives $\psi_{\sigma^2}(h) = (1 - e^{-2h})/2$ and $A_{\text{heat}}(h) = \frac{1+e^{-2h}}{2}e^h = \cosh h > 1$ for all $h > 0$: no step is E1-nonexpansive, and since $\log \cosh$ is convex, $\prod_n \cosh h_n \geq [\cosh(\Lambda/N)]^N \rightarrow \infty$ as $\sigma_{\min} \rightarrow 0$ for fixed N ; no heat mesh is residual-AP. On the uniform mesh $\sigma_n^2 = \sigma_{\max}^2 - n\Delta$, $\Delta = (\sigma_{\max}^2 - \sigma_{\min}^2)/N$, the normal x -factor is $G_n = (\sigma_n^2 + \sigma_{n+1}^2)/(2\sigma_n^2)$. Numbering from the bottom and letting $\sigma_{\min} \rightarrow 0$, $\sigma_m^2 \rightarrow m\Delta$, $G_m \rightarrow 1 - \frac{1}{2m}$, so

$$\text{std}_\perp(x_N) \rightarrow \sigma_{\max} \prod_{m=1}^N \left(1 - \frac{1}{2m}\right) = \sigma_{\max} \frac{(2N-1)!!}{(2N)!!} = \sigma_{\max} \frac{\binom{2N}{N}}{4^N} \sim \frac{\sigma_{\max}}{\sqrt{\pi N}} = \sqrt{\frac{\Delta}{\pi}}$$

by Wallis' asymptotics: the sampler stalls a distance $\sigma_{\max}/\sqrt{\pi N}$ from the data, independent of σ_{\min} , so $W_2 \leq \text{tol}$ forces $N \gtrsim \sigma_{\max}^2/(\pi \text{tol}^2)$. \square

Proposition 4 (flow-matching layer-exactness). On a normal coordinate the data component vanishes, so $X_t = \sigma_t Z$ and the noise posterior is exact, $\eta = \mathbb{E}[Z | X_t] = X_t/\sigma_t = Z$. By equation 5 the velocity reduces to $v_t = \dot{\alpha}_t \mathbb{E}[X_0 | X_t] + \dot{\sigma}_t \eta = \dot{\sigma}_t Z$. A frozen-velocity Euler step gives $X_{t+\Delta t} = X_t + \Delta t \dot{\sigma}_t Z$, while the exact solution is $X_{t+\Delta t} = \sigma_{t+\Delta t} Z$; the two agree for every step iff $\sigma_{t+\Delta t} - \sigma_t = \Delta t \dot{\sigma}_t$, i.e. iff σ_t is affine in t . The gauge α_t only rescales the coordinate and cancels. \square

C PROOF OF THEOREM 3 (TANGENTIAL COVARIANCE LOSS)

On a tangential coordinate ($c > 0$) the exact terminal law is $\mathcal{N}(0, c + \sigma_{\min}^2)$; σ -clock/DDIM sends a centred Gaussian to a centred Gaussian of standard deviation $\rho = \prod_n \rho_n$ times the exact one. One-sidedness is Cauchy-Schwarz: $(c + \sigma_n^2)(c + \sigma_{n+1}^2) - (c + \sigma_n \sigma_{n+1})^2 = c(\sigma_n - \sigma_{n+1})^2 \geq 0$, so $\rho_n \leq 1$. Set $y_n = \log(\sigma_n^2/c)$, $F(y) = \frac{e^y}{(1 + e^y)^2} = \frac{1}{4 \cosh^2(y/2)}$, and $u_n = \sigma_n \sigma_{n+1}/c = e^{\bar{y}_n}$ with $\bar{y}_n = \frac{1}{2}(y_n + y_{n+1})$, $\ell_n = y_n - y_{n+1} = 2h_n$. Writing $\sigma_n = \sqrt{cu_n} e^{h_n/2}$, $\sigma_{n+1} = \sqrt{cu_n} e^{-h_n/2}$ gives $c(\sigma_n - \sigma_{n+1})^2 = 4c^2 u_n \sinh^2(h_n/2)$ and $(c + \sigma_n \sigma_{n+1})^2 = c^2(1 + u_n)^2$, so

$$-\log \rho_n = \frac{1}{2} \log \left(1 + 4 \sinh^2\left(\frac{h_n}{2}\right) \frac{u_n}{(1+u_n)^2}\right) \leq 2 \sinh^2\left(\frac{h_n}{2}\right) F(\bar{y}_n),$$

using $\log(1 + z) \leq z$ and $u_n/(1 + u_n)^2 = F(\bar{y}_n)$. For $h_n \leq h \leq 1$, $2 \sinh^2(h_n/2) = \frac{h_n^2}{2} + O(h_n^4) = \frac{h_n}{4} \ell_n + O(h^2) \ell_n \leq \frac{h}{4} \ell_n + O(h^2) \ell_n$, hence $-\log \rho \leq (\frac{h}{4} + O(h^2)) \sum_n \ell_n F(\bar{y}_n)$.

As \bar{y}_n is the midpoint of $[y_{n+1}, y_n]$, $\int_{\mathbb{R}} F = 1$, and F has bounded variation, the midpoint rule gives $\sum_n \ell_n F(\bar{y}_n) \leq 1 + O(h)$ uniformly in c, σ_{\min} (point clustering cannot inflate a quadrature of a fixed unit-mass integrand). Thus $0 \leq -\log \rho \leq h/4 + O(h^2)$. Sharpness: for $\sigma_{\min}^2 \ll c \ll \sigma_{\max}^2$ and $h_n \equiv h$, $\sum_n u_n / (1 + u_n)^2 \rightarrow \frac{1}{2h} \int_0^\infty (1 + u)^{-2} du = \frac{1}{2h}$, so $-\log \rho \rightarrow \sinh^2(h/2)/h = h/4 + O(h^3)$. Finally, numerical variance = $\rho_i^2 \times \text{exact}$, and normal directions are exact, so $W_2^2(\text{Law}(x_N), p_{\sigma_{\min}}) = \sum_{i:c_i > 0} (1 - \rho_i)^2 (c_i + \sigma_{\min}^2)$, which is Corollary 3. \square

D PROOFS FOR SECTION 5

Proposition 5 (layer geometry). $D_x = s \operatorname{sech}^2 \theta$, so $D_x \geq 1 \iff \cosh \theta \leq \sqrt{s}$, i.e. $|\theta| \leq \operatorname{arccosh} \sqrt{s} = \log(\sqrt{s} + \sqrt{s-1}) = \frac{1}{2} \log(4s) + o(1)$. As $\theta = mx/\sigma^2$, the physical half-width is $w = \frac{\sigma^2}{m} \operatorname{arccosh} \sqrt{s} = \frac{\sigma^2}{2m} \log(4m^2/\sigma^2)(1 + o(1))$, which is equation 25. Near $x = 0$ both mixture components have density $\frac{1}{2}(2\pi\sigma^2)^{-1/2} e^{-m^2/2\sigma^2}$, and $m^2/2\sigma^2 = \Delta^2/8\sigma^2$, so the layer mass is $\asymp \frac{\sigma}{\Delta} \log \frac{\Delta^2}{\sigma^2} e^{-\Delta^2/8\sigma^2}$; the residence time follows from the in-layer escape rate $D_x - 1$, giving $O(1/s)$. From equation 24 with $s \gg 1$, $|D_\lambda \eta| \approx \frac{m}{\sigma} s \operatorname{sech}^2 \theta |\tanh \theta|$; maximizing $g = \operatorname{sech}^2 \theta \tanh \theta = (1 - t^2)t$ in $t = \tanh \theta$ gives $t_* = 1/\sqrt{3}$, $g_* = \frac{2}{3\sqrt{3}}$, and $m/\sigma = \sqrt{s}$, so $\sup_x |D_\lambda \eta| = \frac{2}{3\sqrt{3}} s^{3/2} (1 + O(s^{-1}))$ at $\theta_* = \operatorname{arctanh}(1/\sqrt{3})$. The $\sigma \rightarrow 0$ flow map is $T(x) = m \operatorname{sign}(x)$, discontinuous. \square

Theorem 4 (deterministic no-log). By dimensional analysis \mathcal{M}_{\det} depends only on s ; under the $+m$ component $\theta = s + \sqrt{s}Z$, $Z \sim \mathcal{N}(0, 1)$, and $|D_\lambda \eta|^2 = s \operatorname{sech}^4 \theta (\theta + s \tanh \theta)^2$, so $\mathcal{M}_{\det}(s) = s \mathbb{E}_Z [\operatorname{sech}^4 \theta (\theta + s \tanh \theta)^2]$ (symmetrized). For $s \ll 1$ the mixture is a single Gaussian of variance m^2 and \mathcal{M}_{\det} reduces to the surrogate $s^2/(1+s)^3$; with $d\lambda = ds/2s$,

$$\int_0^\infty \frac{s^2}{(1+s)^3} \frac{ds}{2s} = \frac{1}{2} \int_0^\infty \frac{s ds}{(1+s)^3} = \frac{1}{2} \cdot \frac{1}{2} = \frac{1}{4}.$$

For $s \gg 1$, $p_\theta(\theta) \approx (2\pi s)^{-1/2} e^{-s/2} e^{\pm \theta}$ near $\theta = O(1)$, $\theta + s \tanh \theta \approx s \tanh \theta$, and symmetrizing the two modes produces a factor $\cosh \theta$ with $\int_{\mathbb{R}} \cosh \theta \tanh^2 \theta \operatorname{sech}^4 \theta d\theta = \int_{\mathbb{R}} \tanh^2 \theta \operatorname{sech}^3 \theta d\theta = \frac{\pi}{2} - \frac{3\pi}{8} = \frac{\pi}{8}$, so $\mathcal{M}_{\det}(s) = \frac{\sqrt{\pi/2}}{8} s^{5/2} e^{-s/2} (1 + O(s^{-1}))$. Hence using $\int_0^\infty s^{3/2} e^{-s/2} ds = \Gamma(\frac{5}{2}) 2^{5/2} = 3\sqrt{2}\pi$,

$$\int_0^\infty \mathcal{M}_{\det} d\lambda = \frac{\sqrt{\pi/2}}{16} \int_0^\infty s^{3/2} e^{-s/2} ds = \frac{\sqrt{\pi/2}}{16} \cdot 3\sqrt{2}\pi = \frac{3\pi}{16}.$$

and the density $\propto s^{5/2} e^{-s/2}$ peaks at $s_* = 5$, i.e. $\sigma_* = \Delta/(2\sqrt{5})$. Thus the matched-asymptotic decomposition gives $\frac{1}{4} + \frac{3\pi}{16} \approx 0.84$, while direct quadrature of the exact \mathcal{M}_{\det} gives $\mathfrak{C} \approx 1.01$; either way $\mathfrak{C} = O(1)$, independent of $m, \sigma_{\max}, \sigma_{\min}$. To convert to W_2 : DDIM is order-preserving, $dx_{n+1}/dx_n = e^{-h} + (1 - e^{-h})D_x > 0$ since $D_x = \operatorname{Var}[x_0 | x]/\sigma^2 \geq 0$, so numerical and exact pushforwards of the common base measure are monotone and $W_2^2 = \|T_{\text{num}} - T_{\text{exact}}\|_{L^2(p_{\sigma_{\max}})}^2$ with no coupling loss; and $D(0, \sigma) = 0$ makes $x = 0$ a shared fixed point, so both flows commit to the same basin (no misclassification channel). The residual error is intra-basin discretization plus the exponentially small layer, both bounded by \mathfrak{C} , giving the σ_{\min} -independent $O(h)$ rate with no $\log(1/\sigma_{\min})$. \square

E THE STOCHASTIC BILL AND THE ASYMMETRIC WATERSHED

Cost of freezing η versus D (§5). The Itô budget of Corollary 4, $\frac{1}{D} \mathbb{E} \|I - J_D\|_{\mathbb{F}}^2$, is what an EM/ancestral update pays for freezing the residual η ; the coefficient depends on the frozen object. A frozen- D exponential-SDE update replaces $I - J_D$ by J_D and pays the spectral complement $\frac{1}{D} \mathbb{E} \|J_D\|_{\mathbb{F}}^2$, so the two scalar-preconditioned families fail on complementary directions: η -prediction on directions already committed ($J_D \rightarrow 0$), x_0 -prediction on active data directions ($J_D \rightarrow I$). A v -prediction, or any scalar $c_{\text{skip}}(\sigma)$ interpolation, cancels both only where

$J_D \approx \alpha(\sigma)I$ is scalar; once the posterior spectrum is anisotropic or multiscale a residual martingale cost survives, controlled by the spectral spread of J_D . Freezing instead the full local linearization $D_n + J_D(x_n)(x - x_n)$ —a Rosenbrock-exponential step—cancels the leading martingale and returns the budget to Hessian order; a practical realization is left to future work.

Asymmetric watershed (§5). Unequal weights w_{\pm} on $\pm m$ bias the denoiser to $D = m \tanh(\theta + b)$ with $b = \frac{1}{2} \log(w_+/w_-)$, so the symmetric model of §5 is the case $b = 0$. For $b \neq 0$ the watershed drifts to $x_*(\sigma) = -b\sigma^2/m(1 + O(s^{-1}))$, inside the layer, where the error density is self-correcting, $O(1/s)$, so the deterministic error accumulates only over the commitment window $s = O(1)$. By DDIM monotonicity $W_2^2 = \|T_{\text{num}} - T_{\text{exact}}\|_{L^2(p_{\sigma_{\text{max}}})}^2$ still holds, with basin misallocation moving a quantile mass $\Delta F_* = \kappa(b)h + O(h^2)$ across the gap Δ , where $\kappa(b)$ is a signed integral over the commitment window. If $\kappa(b) \neq 0$ this $O(h)$ mass displaced by $O(\Delta)$ gives W_2 error of order $h^{1/2}$; if $\kappa(b) = 0$ the first-order rate survives. Deciding the sign of $\kappa(b)$ is a one-dimensional quadrature and the only open point for deterministic nonsymmetric mixtures. Stochastic samplers are immune: reinjection resamples the basin at the cost of the Itô budget of Corollary 4.

F THE TWO-MOMENT CHURN INVERSION (§6)

For EDM churn, $\hat{\sigma} = (1 + \gamma)\sigma$ and $\hat{x} = x + \sqrt{\hat{\sigma}^2 - \sigma^2} S_{\text{noise}} z$; the induced jump in η has two orthogonal pieces—a deterministic dilation from re-evaluating at $\hat{\sigma}$, and a stochastic injection through $I - J_D$ —so

$$\frac{\mathbb{E}\|\Delta\eta\|^2}{\dim \cdot \Delta \lambda_{\text{churn}}} = c_{\text{dil}}(\gamma) \mathbf{m}_1 + r(\gamma) S_{\text{noise}}^2 \mathcal{M}_1, \quad \mathbf{m}_1 = \frac{1}{D} \mathbb{E}\|\eta\|^2, \quad \mathcal{M}_1 = \frac{1}{D} \mathbb{E}\|I - J_D\|_{\text{F}}^2. \quad (29)$$

For the full-strength run ($\gamma = \sqrt{2} - 1$, $S_{\text{noise}} = 1.003$) the coefficients are $c_{\text{dil}} = 0.2475$ and $r S_{\text{noise}}^2 = 1.4514$, so $\mathbf{m}_1 \approx \mathcal{M}_1 \approx 1$ predicts 1.699. An EM/ancestral update instead exposes \mathcal{M}_1 in the completed step, up to the finite-step factor $(e^{2h} - 1)/2h$.

G PREDICTIVE-AUDIT PROTOCOL; THE FROZEN AND FLOW BUDGETS

Stage 0 measures the pilot spectra once on the checkpoint of §6: $\mathcal{M}_1(\sigma)$ by the same- σ Gaussian kick equation 9 in its Frobenius form (Remark 1), and $\mathcal{M}_{\text{det}}(\sigma)$ by centered finite differences of η along the exact flow, on a 40-point λ -grid over $\sigma \in [0.002, 80]$, from 256 forward-noised CIFAR-10 training states. Held-out budgets use seeds 1000–1127, disjoint from the pilot states; each configuration logs the dense-substep quantities entering Definition 2(b) to a single archive read by the analyzer, and all predictions are assembled from the Stage-0 spectra alone, the per-step laws equation 13 summed over each candidate mesh and noise level. Each held-out budget carries a standard error over the disjoint seeds (`e2_se`), about 0.5% of the budget, so a 95% normal interval is roughly $\pm 1\%$; the reported relative errors exceed it, so the residuals are systematic rather than sampling noise. A full nonparametric bootstrap over the logged per-trajectory substep records is left to future work. Each configuration fits on a single 24 GB GPU; the campaign was parallelized over two. The reported predictions are the $O(h)$ -corrected refined per-step sums; the leading-order mesh laws equation 14 agree within the same tolerances. The pilot archive stores `lam, sigma, Mdet, Mdet_se, M1, M1_se, m1, cross`; each held-out archive stores `lam_nodes, sigma_nodes, beta, e2, e2_se, e2_per_step, eta_node_norm, n_traj, m_substeps, seeds`, and the dense-substep triples (`sub_sigma_a, sub_sigma_b, sub_na, sub_nb, sub_dot`).

Two stochastic budgets appear, and they are not interchangeable. $\mathcal{E}_2^{\text{flow}}$ evaluates the increments of equation 7 along the true reverse dynamics equation 4 at dense substeps—the marginal-faithful object the mesh laws equation 14 price, and the primary evidence of Figure 3. $\mathcal{E}_2^{\text{frozen}}$ evaluates them along the sampler’s own frozen-drift process—the object Girsanov converts to path-KL in equation 15. Measured, $\mathcal{E}_2^{\text{frozen}}/\mathcal{E}_2^{\text{flow}} - 1$ is +87.3%, +11.6%, +3.1%, +2.3%, +1.1% at $N = 16, 32, 64, 128, 256$: roughly $(0.2\text{--}0.35)h$ for $N \geq 32$, and larger at the coarsest mesh, where $h = \Lambda/16 \approx 0.66$ is not small—consistent with the $O(h)$ numerical-path substitution recorded in Corollary 1(b). The mesh-law gates of Figure 3 are read on $\mathcal{E}_2^{\text{flow}}$ only; $\mathcal{E}_2^{\text{frozen}}$ enters as the KL-facing companion.

Table 3: Clocks and conventions. Our σ -clock follows EDM; the λ -clock is the VE *half* log-SNR of the exponential-integrator solvers. The last column names the variable each family regresses; by Tweedie and equation 5 all are affine repackagings of the one denoiser D —in particular a score target is realized in practice through a scaled noise prediction, since the bare score is stiff as $\sigma \rightarrow 0$.

clock	time	direction	regression target	origin
σ -clock (ours)	σ	$\sigma_{\max} \rightarrow \sigma_{\min}$	denoiser D / x_0	Karras et al. (2022)
λ , half-log-SNR	$\lambda = \log(\sigma_{\max}/\sigma)$	increasing to data	η / D	Lu et al. (2022)
heat (VE)	σ^2	$\sigma_{\max}^2 \rightarrow \sigma_{\min}^2$	$\eta /$ scaled score	Song et al. (2020b)
FM interpolant	t , via $\sigma = \sigma_t/\alpha_t$	$0 \rightarrow 1$	velocity v_t	Lipman et al. (2022)

H A NEGATIVE GATE: THE LEDGER OPTIMUM IS NOT FID-OPTIMAL

The scalar frozen-Jacobian step family (interpolating the frozen- D exponential-SDE step at $c = 0$ and the λ -exact endpoint at $c = 1$) carries a ledger minimizer $c^*(\sigma) = 1 - \mathfrak{m}_1(\sigma)$, the scalar minimizing the frozen-Jacobian Girsanov bill $\mathbb{E}(\nu - c)^2$. A CIFAR-10 pilot on the checkpoint of §6 (2048 images, 35 steps, Karras $\rho = 7$, final denoise, EDM `fid.py` against the CIFAR-10 reference) sampled constant- c members and the measured $c^*(\sigma)$ schedule:

member	description	FID (2048)
$c = 1$	λ -exact endpoint	21.11
$c = 0.5$	constant	24.23
$c = 0$	frozen- D exp-SDE	24.71
$c^*(\sigma)$	ledger minimizer	26.28
$c = 0.25$	constant	26.37

The ledger-minimizing c^* is *not* FID-optimal; the best-FID member is the λ -exact $c = 1$. Because c also changes the injected noise in this one-parameter ($\beta = 1$) family, the pilot does not isolate the ledger-FID relationship, and a decoupled (β, c) study is left to future work. The gate’s role is negative: minimizing the scalar ledger need not improve perceptual quality, which is why the audit claims no sampler improvement.

I DEFERRED COROLLARY PROOFS

Proof of Corollary 2. By Lemma 1 and $d\lambda = -d\sigma/\sigma$, along the exact flow $D_\lambda \eta_i = -\sigma c_i x_i / (c_i + \sigma^2)^2$; squaring and $\mathbb{E}_{p_\sigma} x_i^2 = c_i + \sigma^2$ give equation 20, whose u -derivative $(1 - 2u_i)/(1 + u_i)^4$ vanishes at $u_i = \frac{1}{2}$. Per coordinate $d\lambda = du/(2u)$ and $\int_0^\infty (1 + u)^{-3} du = \frac{1}{2}$; the finite endpoints contribute the stated corrections. \square

Proof of Corollary 4. $J_D = C(C + \sigma^2 I)^{-1}$ is symmetric (§4), so the Frobenius mass equation 8 is the eigenvalue sum of $(I - J_D)^2$: normal coordinates contribute 1 each, tangential ones $(u_i/(1 + u_i))^2 \leq \min(1, u_i^2)$, giving equation 27 and the plateau on $\sigma_{\min} \leq \sigma \leq \sqrt{c_d}$, a λ -interval of length $\Lambda - O(1)$. Integrating with $d\lambda = du/(2u)$ per coordinate, $\int u du/2(1 + u)^2 = \frac{1}{2} \log(1 + u) + \frac{1}{2}(1 + u)^{-1}$, so each tangential coordinate adds at most $\frac{1}{2} \log(\sigma_{\max}^2/c_i) + O(1)$, independent of σ_{\min} . On a committed mixture direction $D_x = s \operatorname{sech}^2 \theta \rightarrow 0$ exponentially in s off the layer (Proposition 5), so $\mathcal{M}_1 \rightarrow 1$. The displays follow from equation 14 and equation 15 at $\beta = 1$; the deterministic rate is Corollary 1(b). \square

J EXTENDED REMARKS

Three readings of the Gaussian budget (§4.2). We derive the three assertions recorded after Corollary 1. *First*, the theorem and the corollary give the same $\frac{1}{4}$ from the same λ -octave. Both are λ -integrals of octave-local densities in $y = \log(\sigma^2/c_i)$: the scheme’s one-sided defect weighs the transition profile $u/(1 + u)^2$, of unit y -mass, by its Taylor factor $2 \sinh^2(h/2) \approx h^2/2$ (Appendix C);

the flow's own squared velocity equation 20 is the tilted profile $u/(1+u)^3$, of y -mass exactly one half. With the common Jacobian $d\lambda = \frac{1}{2} dy$, both ledgers close at $\frac{1}{4}$ —the scheme's, retaining one factor of the step, as the theorem's $h/4$; the flow's, step-free, as the budget's per-coordinate $\frac{1}{4}$. *Second*, the peak at $\sigma^2 = c_i/2$ makes the band concentration quantitative: the deterministic ledger charges only the spectral band $[\sqrt{c_d}, \sqrt{c_1}]$, which is all a schedule must resolve (Remark below). *Third*, the same constant appears in both models. Under the inversion $u = 1/s$ the per-coordinate density $du/2(1+u)^3$ transforms exactly into $s ds/2(1+s)^3$ —the $s \ll 1$ Gaussian-core surrogate of the mixture budget in Theorem 4—so the $\frac{1}{4}$ of the mixture's $\frac{1}{4} + \frac{3\pi}{16}$ is this same coordinate integral read at $c = m^2$: the Gaussian core appears in both models because both reduce to one coordinate integral under this change of variables.

Relation to classical a posteriori estimation. The audit is a posteriori in the classical sense—residual-based, computed from the numerical solution, requiring no exact one—in the lineage of embedded error estimators in ODE codes (Hairer et al., 1993), residual indicators in finite elements (Verfürth, 1996), and, on the diffusion side, adaptive SDE solvers (Jolicœur-Martineau et al., 2021). What is new is where the estimates must hold: classical indicators control error in h at fixed regularity, and their constants degenerate exactly where diffusion sampling lives, the score's Lipschitz constant being σ_{\min}^{-2} (§1). The defining requirement here is uniformity in the singular parameter: every functional in Definition 2 carries $O(1)$ coefficients as $\sigma_{\min} \rightarrow 0$, and Theorem 1(iii) shows this is a structural property of the chart: the audit must be conducted in the micro variable η (equivalently any bounded repackaging), never in the bare score. In the vocabulary of Definition 1, the *estimates* commute with the singular limit, as the schemes must: asymptotic-preserving a posteriori estimation. The named constants of §4–5— $h^* = 1 + W(1/e)$, the Wallis floor, $\frac{1}{4}$, $\frac{3\pi}{16}$ —are then not only sharpness certificates for schemes; they calibrate the audit itself, on models where every functional is closed-form.